NASA/TM—2010-216735 AIAA–2010–578

Comparing Spray Characteristics from Reynolds Averaged Navier-Stokes (RANS) National Combustion Code (NCC) Calculations Against Experimental Data for a Turbulent Reacting Flow

Anthony C. Iannetti and Jeffery P. Moder
Glenn Research Center, Cleveland, Ohio

July 2010

NASA STI Program . . . in Profile

Since its founding, NASA has been dedicated to the advancement of aeronautics and space science. The NASA Scientific and Technical Information (STI) program plays a key part in helping NASA maintain this important role.

The NASA STI Program operates under the auspices of the Agency Chief Information Officer. It collects, organizes, provides for archiving, and disseminates NASA's STI. The NASA STI program provides access to the NASA Aeronautics and Space Database and its public interface, the NASA Technical Reports Server, thus providing one of the largest collections of aeronautical and space science STI in the world. Results are published in both non-NASA channels and by NASA in the NASA STI Report Series, which includes the following report types:

- TECHNICAL PUBLICATION. Reports of completed research or a major significant phase of research that present the results of NASA programs and include extensive data or theoretical analysis. Includes compilations of significant scientific and technical data and information deemed to be of continuing reference value. NASA counterpart of peer-reviewed formal professional papers but has less stringent limitations on manuscript length and extent of graphic presentations.

- TECHNICAL MEMORANDUM. Scientific and technical findings that are preliminary or of specialized interest, e.g., quick release reports, working papers, and bibliographies that contain minimal annotation. Does not contain extensive analysis.

- CONTRACTOR REPORT. Scientific and technical findings by NASA-sponsored contractors and grantees.

- CONFERENCE PUBLICATION. Collected papers from scientific and technical conferences, symposia, seminars, or other meetings sponsored or cosponsored by NASA.

- SPECIAL PUBLICATION. Scientific, technical, or historical information from NASA programs, projects, and missions, often concerned with subjects having substantial public interest.

- TECHNICAL TRANSLATION. English-language translations of foreign scientific and technical material pertinent to NASA's mission.

Specialized services also include creating custom thesauri, building customized databases, organizing and publishing research results.

For more information about the NASA STI program, see the following:

- Access the NASA STI program home page at *http://www.sti.nasa.gov*

- E-mail your question via the Internet to *help@sti.nasa.gov*

- Fax your question to the NASA STI Help Desk at 443–757–5803

- Telephone the NASA STI Help Desk at 443–757–5802

- Write to:
  NASA Center for AeroSpace Information (CASI)
  7115 Standard Drive
  Hanover, MD 21076–1320

NASA/TM—2010-216735 AIAA–2010–578

Comparing Spray Characteristics from Reynolds Averaged Navier-Stokes (RANS) National Combustion Code (NCC) Calculations Against Experimental Data for a Turbulent Reacting Flow

Anthony C. Iannetti and Jeffery P. Moder
Glenn Research Center, Cleveland, Ohio

Prepared for the
48th Aerospace Sciences Meeting
sponsored by the American Institute of Aeronautics and Astronautics
Orlando, Florida, January 4–7, 2010

National Aeronautics and
Space Administration

Glenn Research Center
Cleveland, Ohio 44135

July 2010

Acknowledgments

We would like thank to Dan Bulzan, Yolanda Hicks, Nan-Suey Liu, and Mathena Suri Raju for their valuable advice. This work was funded by the Subsonic Fixed Wing and Supersonic Fixed Wing programs in Aeronautics Research Mission Directorate. High Performance Computing (HPC) resources were provided by the NASA Advanced Supercomputer division at NASA Ames Research Center. We also wish to acknowledge the support of the Graphics and VISualization (G-VIS) lab at NASA Glenn.

This work was sponsored by the Fundamental Aeronautics Program at the NASA Glenn Research Center.

Level of Review: This material has been technically reviewed by technical management.

Available from

NASA Center for Aerospace Information
7115 Standard Drive
Hanover, MD 21076–1320

National Technical Information Service
5301 Shawnee Road
Alexandria, VA 22312

Available electronically at http://gltrs.grc.nasa.gov

Contents

List of Tables

List of Figures

Comparing Spray Characteristics from Reynolds Averaged Navier-Stokes (RANS) National Combustion Code (NCC) Calculations Against Experimental Data for a Turbulent Reacting Flow

Anthony C. Iannetti and Jeffery P. Moder
National Aeronautics and Space Administration
Glenn Research Center
Cleveland, Ohio 44135

Abstract

Developing physics-based tools to aid in reducing harmful combustion emissions, like Nitrogen Oxides (NOx), Carbon Monoxide (CO), Unburnt Hydrocarbons (UHC's), and Sulfur Dioxides (SOx), is an important goal of aeronautics research at NASA. As part of that effort, NASA Glenn Research Center is performing a detailed assessment and validation of an in-house combustion CFD code known as the National Combustion Code (NCC) for turbulent reacting flows. To assess the current capabilities of NCC for simulating turbulent reacting flows with liquid jet fuel injection, a set of Single Swirler Lean Direct Injection (LDI) experiments performed at the University of Cincinnati was chosen as an initial validation data set. This Jet-A/air combustion experiment operates at a lean equivalence ratio of 0.75 at atmospheric pressure and has a 4 percent static pressure drop across the swirler. Detailed comparisons of NCC predictions for gas temperature and gaseous emissions (CO and NOx) against this experiment are considered in a previous work. The current paper is focused on detailed comparisons of the spray characteristics (radial profiles of drop size distribution and at several radial rakes) from NCC simulations against the experimental data. Comparisons against experimental data show that the use of the correlation for primary spray break-up implemented by Raju in the NCC produces most realistic results, but this result needs to be improved. Given the single or ten step chemical kinetics models, use of a spray size correlation gives similar, acceptable results.

Nomenclature

C_p	specific hear with respect to pressure
D_{32}	Sauter Mean Diameter (SMD)
D_{min}	minimum droplet group diameter
D_{max}	maximum droplet group diameter
k	turbulent kinetic energy
P_3	static pressure at combustor inlet
Re_{drop}	liquid phase droplet group Reynolds Number
SMD	Sauter Mean Diameter (SMD), same as D_{32}
T	temperature
$\mathbf{V_{drop}}$	liquid phase droplet group velocity vector
$\mathbf{V_{gas}}$	gas phase velocity vector
$\mathbf{V'_{gas}}$	turbulent fluctuations of the gas phase velocity vector
y^+	non-dimensional turbulent wall boundary layer distance
ε	turbulent dissipation

1.0 Introduction

The use of combustion Computational Fluid Dynamics (CFD) in the development of combustion technology has been greatly facilitated by the advancements made during the last decade in the areas of combustion modeling, numerical simulation, and computing platform. Further development of verification, validation, and uncertainty quantification will profoundly impact the reliability and utility of these modeling and simulation tools. Under the NASA Fundamental Aeronautics Program, an assessment of existing computational tools for emissions and flow field is being carried out. As a first step, the present effort aims at establishing the baseline for prediction methods and experimental data for Lean Direct Injection (LDI) (Refs. 1 to 3) combustion in confined, swirling flows. Combustion codes based on Reynolds Averaged Navier-Stokes (RANS), the Partially Resolved Numerical Simulation method (PRNS, using a two equation sub-grid model), and traditional Large Eddy Simulation (LES) using Smagorinsky type sub-grid approaches will be used; the present paper reports the preliminary investigation using the National Combustion Code (NCC). Currently, NASA is partnering through cooperative agreements with research groups at Stanford (Ref. 4) and Georgia Tech (Ref. 5) Universities to investigate LDI flow fields with LES.

This paper extends the LDI combustion steady-state RANS CFD analysis of Davoudzadeh (Refs. 6 and 7) for non-reacting flow and Iannetti et al., (Ref. 8) for reacting spray calculations. Where Iannetti compared gas phase quantities such a temperature, emissions, and the reacting gas phase flow field, this paper will compare the NCC using a steady-state RANS approach against experimental drop size measurements for a confined, swirling, reacting spray flow. This paper will attempt to provide some insight into whether experimental correlations or more sophisticated, less empirical, break-up models should be used for primary atomization.

2.0 Experimental Data

A detailed description of the experimental hardware, facility, diagnostics and results is given by Jun Cai, S.-M. Jeng, and R. Tacina (Ref. 9), and by Yongqiang Fu and San-Mou Jeng (Ref. 10). Only a brief summary is provided here. The spray measurements used an Aerometrics two-component Phase Doppler Particle Analyzer (PDPA) operated in 30° off-axis forward scatter mode. The transmitting and receiving lenses had focal lengths of 500 and 300 mm. A 3 W Argon laser was used as the light source. The data rate was 300 to 20,000 Hz and an average of 10,000 data points were collected during a 7 sec period at each measurement location. Spray velocity components (axial, radial, and tangential) and drop size distributions were collected at many axial locations, with around thirty-seven radial locations (–12 to 24 mm radially from injector center) at each axial location. The comparisons presented in the current paper focus on axial locations “near” the injector (3, 5, 7, 9, 12, 15, 20, and 25 mm from injector exit face). The experiment is shown in Figure 1.

Measurements at a particular axial and radial location (relative to the injector centerline) by the PDPA system take place in the intersection between the two incident laser beams. The measurement volume is defined here as the volume within which the modulation depth is higher than e^{-2} times the peak core laser intensity value and forms an ellipsoid with an essentially circular cross-section. Jeng, Cai, and Fu, do not provide enough information to calculate ellipsoidal measurement volume for PDPA system, we estimate the laser probe ellipsoidal measurement volume with a minor diameter of 1 mm and a major diameter of 5 mm. In CFD simulations, computational spray data is collected in an ellipsoidal probe volume (with diameters of 1 by 1 by 10 mm) at the same axial and radial locations as the experiment. Figure 2 shows such a PDPA probe volume.

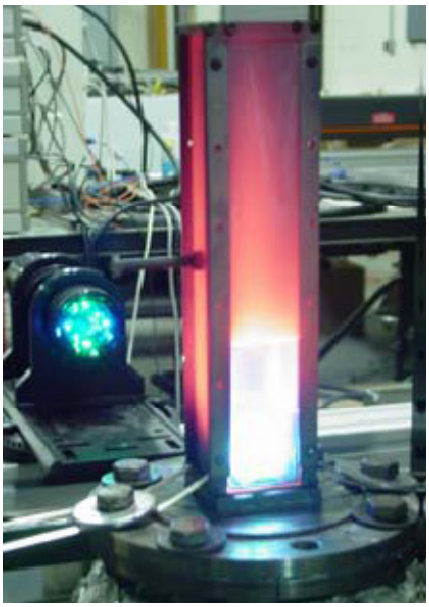

Figure 1.—Picture of the actual single swirler LDI experiment (Cai and Jeng, 2005).

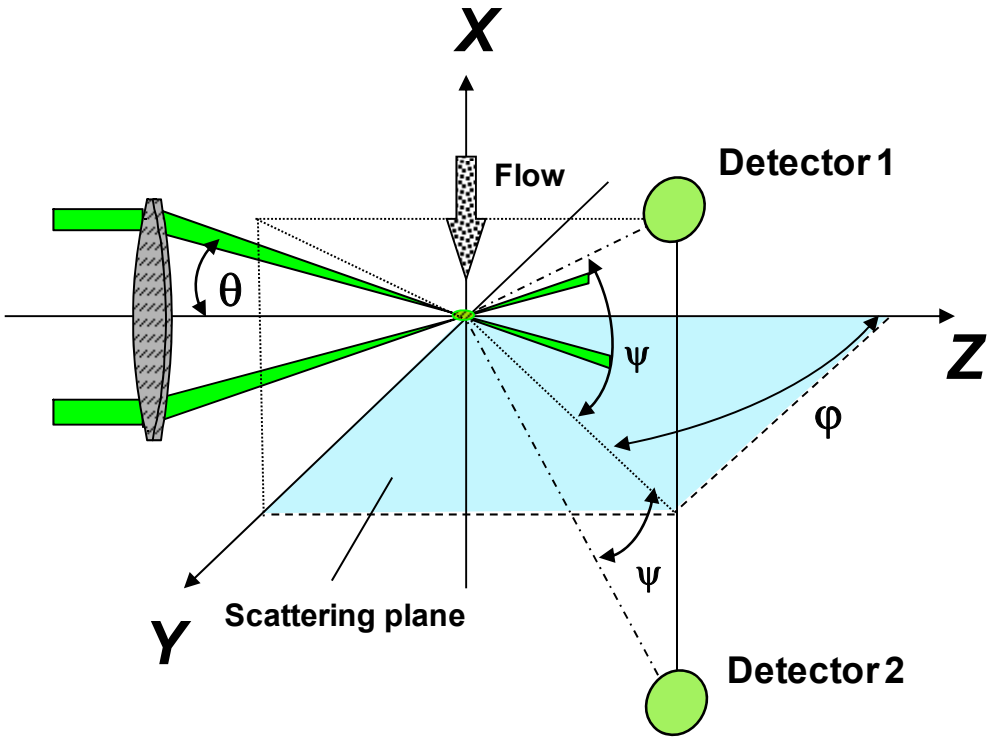

Figure 2.—Overview of a PDPA system, showing the ellipse formed at the beam crossing. (Courtesy: Dantec)

3.0 NCC Simulations

3.1 The National Combustion Code

The National Combustion Code (NCC) is a state of the art CFD program specifically designed for combustion processes. A short summary of the features of the NCC pertaining to this paper are: the use of unstructured grids (Ref. 11), massively parallel computing—with almost perfectly linear scalability (Refs. 12 and 13) on non-spray cases up to four thousand central processing units (CPU), a dynamic wall function with the effect of adverse pressure gradient (Ref. 14), low Reynolds number wall treatment (Ref. 15), and a cubic non-linear k-epsilon turbulence model (Refs. 16 and 17), lagrangian liquid phase spray model (Ref. 18), and stiff laminar chemistry integration. Recently, viscous low-speed preconditioning (Refs. 19 and 20) has been added to improve the low-speed convergence of the NCC in viscous regions, and the ability to handle multiple sets of periodic boundary conditions has also been added. The combination of these features is usually not available in other CFD codes and gives the NCC an advantage when computing recirculating, turbulent, reacting, spray flows. Previously, the NCC has undergone extensive validation studies for simple flows (Ref. 21), complex flows (Ref. 22), NO_x emissions prediction performance (Ref. 23), and traditional gas turbine combustor/injectors (Ref. 24).

3.2 Geometry and Mesh Generation

The single-element LDI swirler configuration is illustrated in Figure 3. Each element consists of an air passage with an upstream air swirler and a converging-diverging venturi section. The fuel is injected through the center of swirler and the fuel tip is at the throat of the venture. The air swirlers have helical, axial vanes with downstream vane angles of 60°. There are six vanes with an inside diameter of 9.3 mm and an outside diameter of 22.1 mm. The air then dumps into a 50.8 by 50.8 mm combustion section.

Since the NCC allows for unstructured elements, the grid may be composed of any type and mix of three-dimensional elements. However, hexahedral elements were chosen because they are more efficient at filling a volume with a smaller number of elements compared to an all tetrahedral grid. Hexahedral elements also allow a better calculation of the normal derivatives that are crucial for accurate boundary layer resolution. Approximately 850,000 elements were used (shown in Fig. 4). Current simulations have y+ values ranging from 0.5 to 45 (non-dimensional) in various parts of the grid. The “Gridgen” mesh generation software was used to create all the grids used in the numerical simulation reported in this paper.

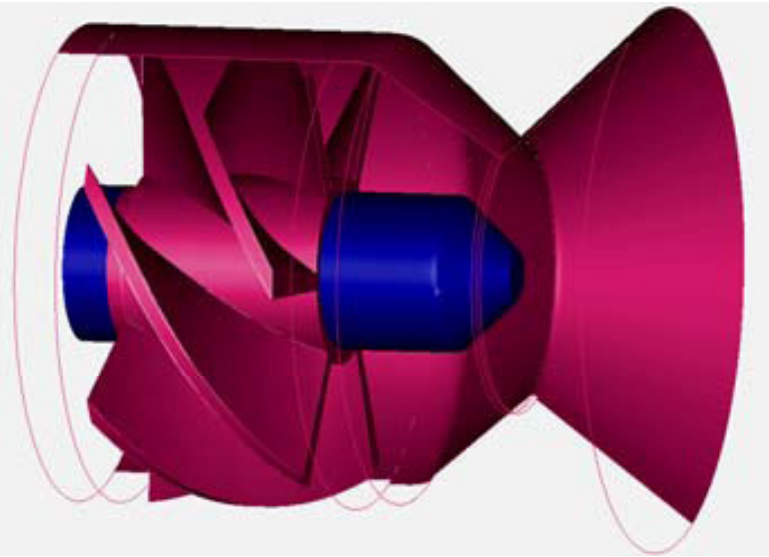

Figure 3.—Single element LDI injector geometry.

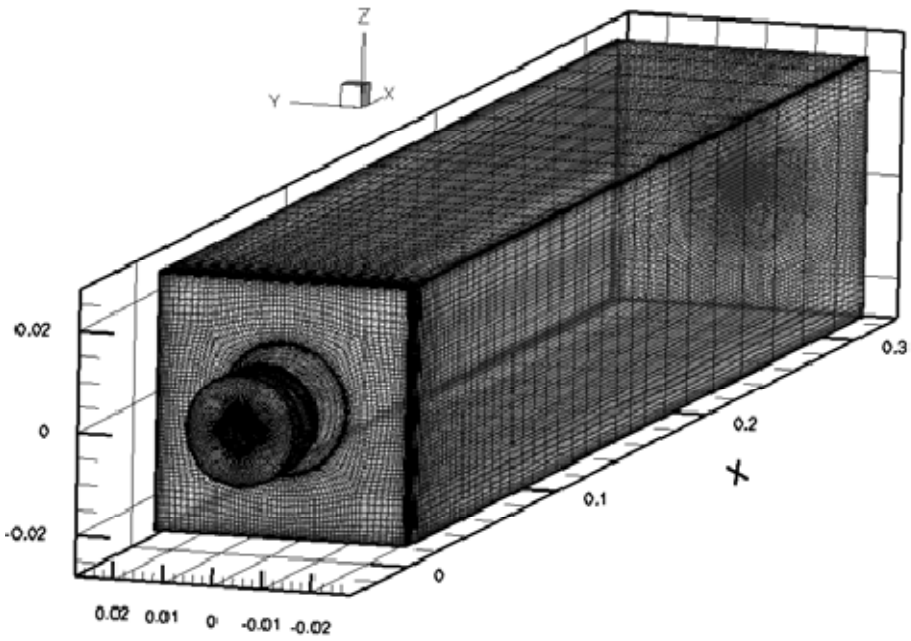

Figure 4.—Computational grid for the single element LDI combustor. The dimensions are in meters.

3.3 Operating Conditions

The gas-phase boundary conditions consist of the inlet to the swirler, the exit of the computational domain, and the walls. All walls are treated as no-slip and adiabatic. The air enters the swirler with uniform values for axial velocity (20.14 m/s), temperature (294.28 K), turbulent kinetic energy (k = 1.521 m^2/s^2) or 5 percent turbulence intensity level, and specific dissipation (ε = 2.015 W/kg). The gas-phase exit boundary condition is a uniform static pressure of 1 atm (101325 Pa), while the equivalence ratio is 0.75. The measured pressure drop (as a percentage of P_3) during the experiments was measured at 4 percent. The fuel nozzle used is a Parker-Hannifin 90°, hollow cone, pressure swirl atomizer which has the flow number of 0.75.

3.4 Chemistry Modeling

Ideally, we would prefer to use detailed chemical kinetic models. There are two problems with this approach: (1) Jet-A is a fuel and not a substance, and there are no universally accepted surrogate fuel models for Jet-A; (2) the computational costs associated with these models make them impractical when fine computational grids are used. Originally, a single-step, global chemistry model was used, shown in Table 1. This model was based on propane kinetics (Ref. 25), which are close to Jet-A's reaction rates. The Jet-A fuel is modeled as single species (C12H23) in both gas-phase and liquid-phase solvers. The gas is treated as ideal mixture with five-coefficient curve fits for C_p (T) of each species and a CHEMKIN treatment of transport properties (species and ideal mixture rules). The single-step model allowed an easier start up in the solution process, by reducing the computational requirements during the ignition phase. Single-step models do not allow emissions calculations, only heat release. Because of this, a reduced ten-step, twelve species model based on propane kinetics (Refs. 26 and 27) was used, as shown in Table 2. The mechanism was developed by a gradual reduction of reaction steps and species using sensitivity techniques. The reduced mechanism also describes the formation of Carbon Monoxide and Nitrogen Oxide. However, only one nitrogen-oxide species, NO, has been used in the reduced mechanism. NO in the reduced mechanism represents the whole family of nitrogen oxides including nitric oxide by Zeldovich (Ref. 28) reactions, prompt NO reactions by Fenimore (Ref. 29), and nitrogen oxide formation through nitrous oxide.

TABLE 1.—SINGLE STEP (GLOBAL) CHEMISTRY MODEL

	Reaction	A (mole – cm – sec– K)	n	E (cal/mole)
1	**4 C12H23 + 71 O2 => 48 CO2 + 46 H2O** *GLO / C12H23 0.10 /* *GLO / O2 1.65 /*	8.60E+11	0.00	3.00E+4

TABLE 2.—REDUCED 10 STEP, 12 SPECIES CHEMISTRY MODEL IN CHEMKIN FORMAT

	Reaction	A (mole – cm – sec – K)	n	E (cal/mole)
1	**4 C12H23 + 47 O2 => 48 CO + 46 H2O** *GLO / C12H23 0.1 /* *GLO / O2 1.6 /*	1.46E+13	0.00	3.40E+4
2	**H2 + O2 <=> H2O + O**	3.98E+11	1.00	4.80E+4
3	**H2 + O <=> H + OH**	3.00E+14	0.00	6.00E+3
4	**H + O2 <=> O + OH**	4.00E+14	0.00	1.80E+4
5	**CO + OH <=> CO2 + H**	1.51E+07	1.28	–7.58E+2
6	**H2O + O2 <=> 2O + H2O**	3.17E+12	2.00	1.12E+5
7	**CO + H2O <=> CO2 + H2**	5.50E+04	1.28	–1.00E+3
8	**N2 + O <=> N + NO**	1.00E+14	0.00	7.50E+4
9	**N + O2 <=> NO + O**	6.30E+09	1.10	6.28E+3
10	**N + OH <=> NO + H**	3.80E+13	0.00	0.00E+0

3.5 Liquid Phase Modeling

The liquid Jet-A spray is evolved using a dilute spray Lagrangian solver4 which neglects any drop-drop interactions. Turbulence effects follow the KIVA-II approach (Ref. 30) of adding a turbulent fluctuation velocity to gas-phase velocity when calculating droplet drag and vaporization. The evaporation model includes solution of internal drop temperature distribution (thirteen point one dimensional mesh, finite-difference solution of a Hill vortex model) and a droplet regression rate employing three different correlations depending on droplet Reynolds number, Re_{drop} (where Re_{drop} is based on the relative speed $\mathbf{V_{gas}} + \mathbf{V'_{gas}} - \mathbf{V_{drop}}$).

Two different primary atomization models and two different secondary break-up models are described below.

3.5.1 Primary Atomization Using a Correlation

The liquid spray injection is modeled using a specified drop size distribution at injector exit face. The specified drop size distribution uses a Sauter Mean Diameter (SMD) of D_{32} = 32 μm and D_{32} = 42 μm, a 3-D hollow cone with a half-cone angle of 14° and 32 circumferential streams leaving the injector. The original SMD of 32 μm for the injection droplet size was based on previous dropsize data and experience with Parker Hannifin *LDI* fuel injectors. A new SMD of 42 μm was based on pressure swirl atomizer correlations from Lefevbre (Ref. 31). Drop size distributions are currently based on a widely used correlation (Ref. 32) but other correlations may be considered. Figure 5 shows the cumulative drop size distribution, the mass fraction of droplets at a given size diameter (the spray initial condition used), from the correlation with a SMD of 32 and 42 μm. The liquid temperature, mass flow rate and drop speed are:

T_{drop} = 300 K
Liquid mass flow rate = 0.415E-03 kg/sec
Drop speed = 20 m/s

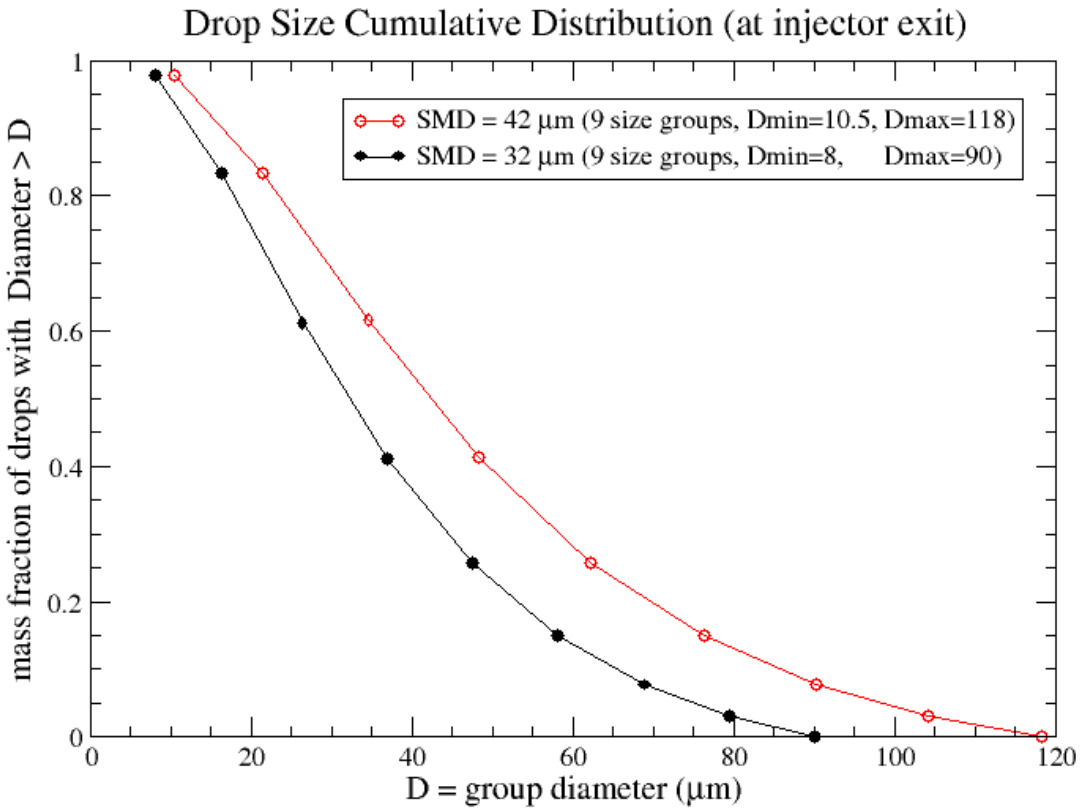

Figure 5.—Cumulative drop size distribution (spray initial condition) from the correlation with a given SMD of 32 and 42 μm.

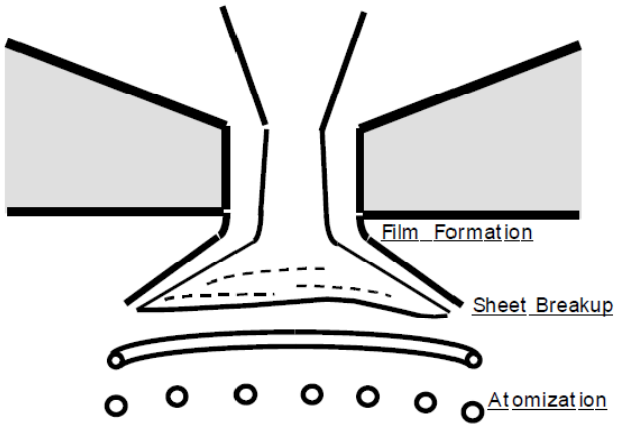

Figure 6.—A sketch of the transition from the internal flow to the external spray (Ref. 33).

3.5.2 Primary Atomization Using a Sheet Break-Up Model

The Liquid Instability Sheet Atomization (LISA) model for primary break-up was used. This was originally formulated by Schmidt et al., (Ref. 33) and refined by Chryssakis et al., (Ref. 34). The LISA mathematical model was coded in Fortran 95 as a module by the company CFDRC (via NASA's Small Business Innovative Research program) and integrated into the NCC by Raju (Ref. 35). Figure 6 shows the primary atomization process assumed in the LISA model. Essentially, a film sheet is produced from the rotating flow inside a pressure swirl atomizer. This then forms ligaments which further tear to form droplets.

3.5.3 Secondary Atomization Models

The Rayleigh-Taylor, a model that describes break-up due to long waves in a decelerating flow, and the Enhanced Taylor Analogy Break-up (ETAB), initially designed for diesel fuel injection and improved version of the Taylor Analogy Break-up (TAB) model, were used to model the secondary atomization that occurs downstream stream of the primary break-up. These are described in detail in Raju.

During all Lagrangian spray integrations in NCC, each spray particle represents a number of actual droplets which for that spray particle are all assumed to behave in the same way and thus have the same drop diameter, internal droplet temperature distribution, and for multi-component drops, the same internal droplet species composition. The sheet break-up atomization model injects a user-defined number of spray particles with each particle having the same drop diameter. When primary atomization occurs, the number of spray particles remains the same, but the drop diameter at break-up is determined by randomly sampling from a predefined drop distribution function. Thus, while the drop size of all injected spray particles was initially the same, as each particle undergoes primary atomization, a distribution of drop sizes results (but the number of spray particles tracked during the simulations remains unchanged). Also, all secondary break-up models in NCC currently only change the drop diameter associated with a given spray particle; no new spray particles are created by any of the secondary break-up models.

3.6 Computational Procedure

The simulations are steady-state and solve the Favre-averaged transport equations for species, momentum and energy, as well as a two-equation k-ε turbulence model. Staging was used in the solution process; cold-flow calculations and initial combustion calculations were performed using a single-step chemistry model with lagrangian spray until a steady state solution was obtained. The final stage of CFD calculations was performed by switching from the one-step chemistry model to the reduced chemistry model; this was done by changing the input chemistry-parameters of the code. It is important to note that no turbulence—chemistry interaction model was used for this case, so called “laminar chemistry”. So, averaged temperature and averaged mass fractions are used to compute the reaction rate. For this case, we believe this an appropriate as an engineering assumption, because for this particular case, turbulent kinetic energy (k) is below 20 m^2/s^2, with the peak occurring at the tip of the fuel injector.

Calculation of the source term due to chemical kinetics uses the explicit “reference species” approach described in the KIVA-II manual. In the current implementation, the explicit “reference species” integration of chemical kinetics source is performed using three sub-iterations within each pseudo-time step of gas-phase Runge-Kutta integration in pseudo-time.

The NCC computations for reacting and non-reacting flow were run in general until the flow residuals were reduced three orders of magnitude. The mass flow rates at the boundary conditions were also monitored as a convergence criterion. Dissipation (JST type) was set at 0.0 for second order dissipation (ε_2) and 0.1 for fourth order dissipation (ε_4) (Ref. 36). The value of k_2, the constant that scales the second order dissipation gradient switch, was set at 0.50. Setting the second order dissipation to zero is absolutely necessary to accurately resolving flow features, like jets. A CFL number of 1.0 was used. A cubic, non-linear k-epsilon model with a variable C_{mu} coefficient was used. This model was selected because of the swirling flow. A dynamic wall function with pressure gradient effects was used to model near wall turbulent flow effects.

Computations were performed on a variety of computer platforms, namely SGI ICE computer “RTJones” at NASA Ames and Linux clusters Glenn. The “RTJones” supercomputer was preferred because it was considerably faster because of its high speed, low-latency interconnect. This interconnect was important because the Lagrangian spray model created a load unbalance in compute nodes. The high speed interconnect seemed to mitigate the load imbalance. It takes approximately one week to complete a single LDI combustion case using 96 processors. After the baseline run was completed, new runs starting from the baseline case took about one to five days depending on the chemistry model and secondary break-up model used.

4.0 Results and Discussion

4.1 Casers Performed

The combustion CFD cases calculated with the NCC are shown in Table 3. A total of twelve cases were performed.

TABLE 3.—CFD CASES PERFORMED

Case	Chemistry model	Primary break-up model	Secondary break-up model
1	Single step	Correlation with 32 μm SMD	Rayleigh-Taylor
2	Single step	Correlation with 32 μm SMD	Enhanced Taylor Analogy Break-up
3	Single step	Correlation with 42 μm SMD	Rayleigh-Taylor
4	Single step	Correlation with 42 μm SMD	Enhanced Taylor Analogy Break-up
5	Ten step	Correlation with 32 μm SMD	Rayleigh-Taylor
6	Ten step	Correlation with 32 μm SMD	Enhanced Taylor Analogy Break-up
7	Ten step	Correlation with 42 μm SMD	Rayleigh-Taylor
8	Ten step	Correlation with 42 μm SMD	Enhanced Taylor Analogy Break-up
9	Single step	Sheet break-up	Rayleigh-Taylor
10	Single step	Sheet break-up	Enhanced Taylor Analogy Break-up
11	Ten step	Sheet break-up	Rayleigh-Taylor
12	Ten step	Sheet break-up	Enhanced Taylor Analogy Break-up

4.2 Comparison of Clip Planes

Clip planes in Figures 7 to 15 attempt to show how the different atomization models affect the overall flow field. Figures 7 to 9 show how the break-up models affect temperature. For the single step kinetics model, very little difference is observed when using the droplet size correlation and the different secondary break-up models. The ten step kinetics models are much more sensitive to the type of secondary atomization models used, probably because of grid density. The overall flame shape is roughly the same. When looking at Figure 9, we observed a dramatically different flame shape from using the correlation for primary atomization. These results indicate the droplet sizes produced by the sheet break-up model are too large. Figures 10 to 12 show the unburnt fuel vapor ($C_{12}H_{23}$, Jet-A). Similar to the temperature contours, little difference is seen when using the correlation with single step kinetics. Using ten step kinetics, we generally see smaller regions of fuel vapor than in the single step case, except for the 42 μm SMD with the ETAB model. The sheet break model produces very small regions of fuel vapor, and regions appear to exist on the sides of the combustor wall. This also indicted large droplet sizes being produced. Figures 13 to 15 qualitatively show that the flow field is not affected by the different atomization models. This indicates that the mean recirculation zone is fairly stable and insensitive to heat release.

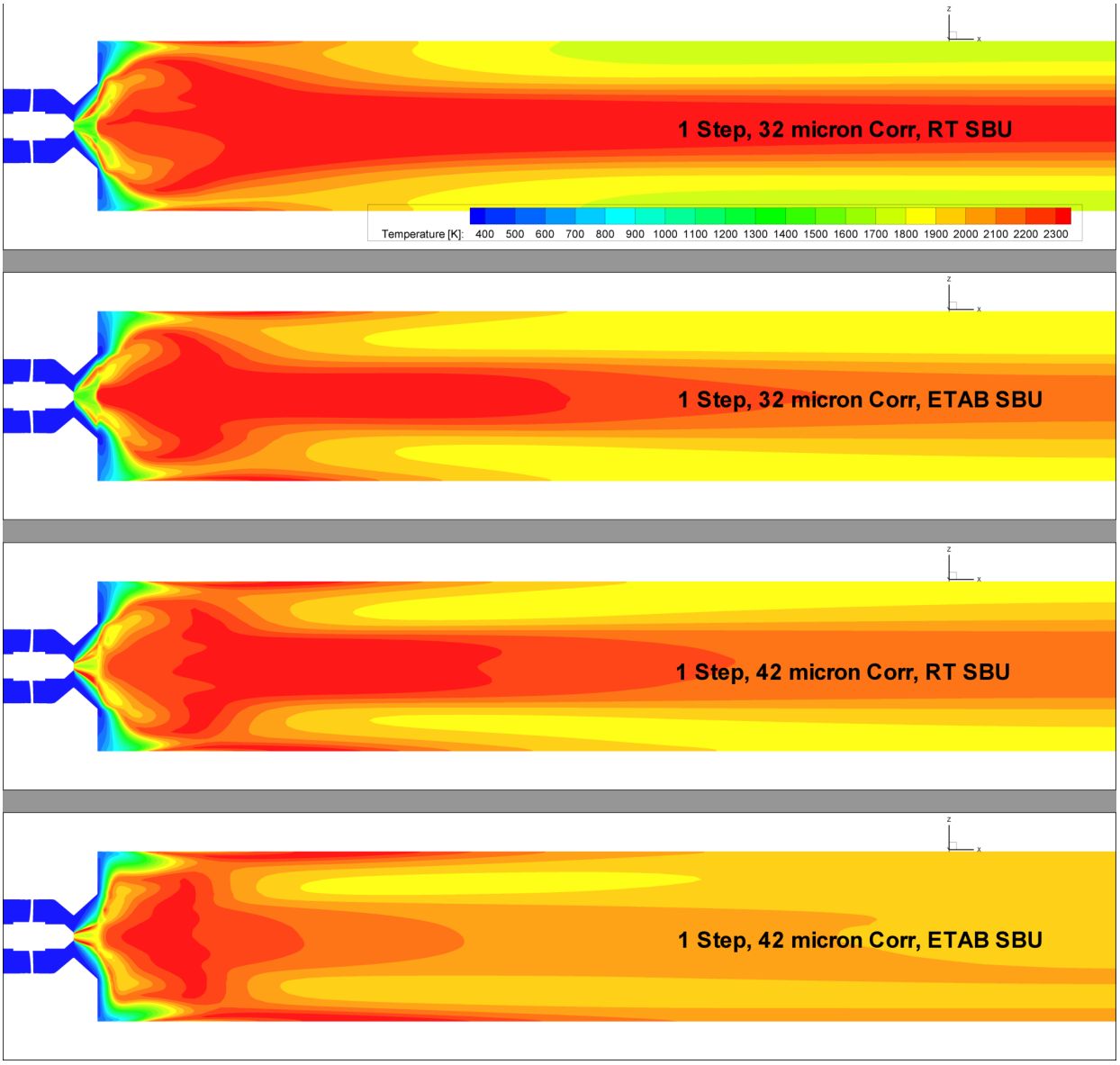

Figure 7.—Contours of temperature [K] using single step chemistry with the atomization correlation for primary break-up and various secondary break-up models at the Y = 0 mm mid-plane.

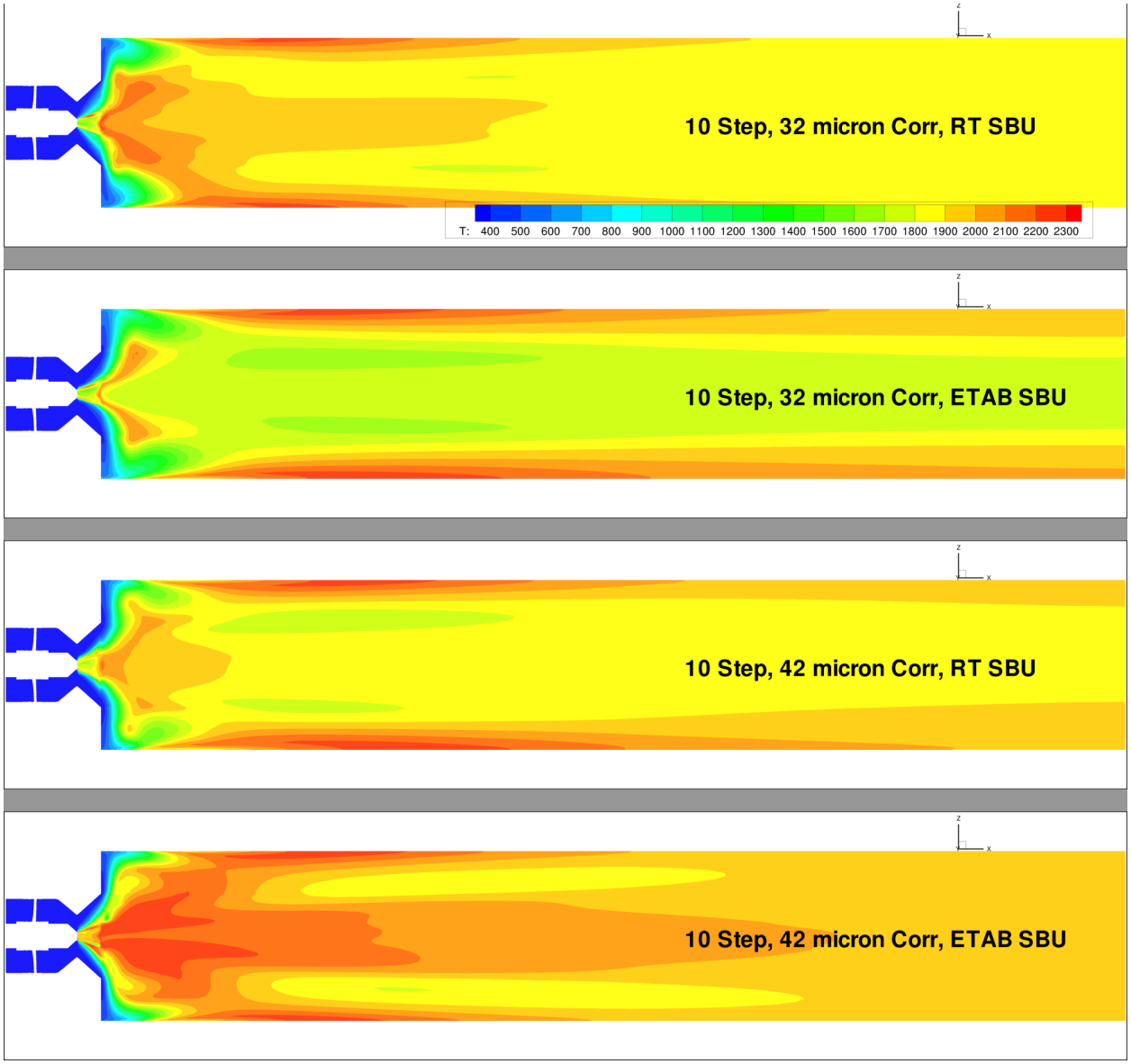

Figure 8.—Contours of temperature [K] using ten step chemistry with the atomization correlation for primary break-up and various secondary break-up models at the Y = 0 mm mid-plane.

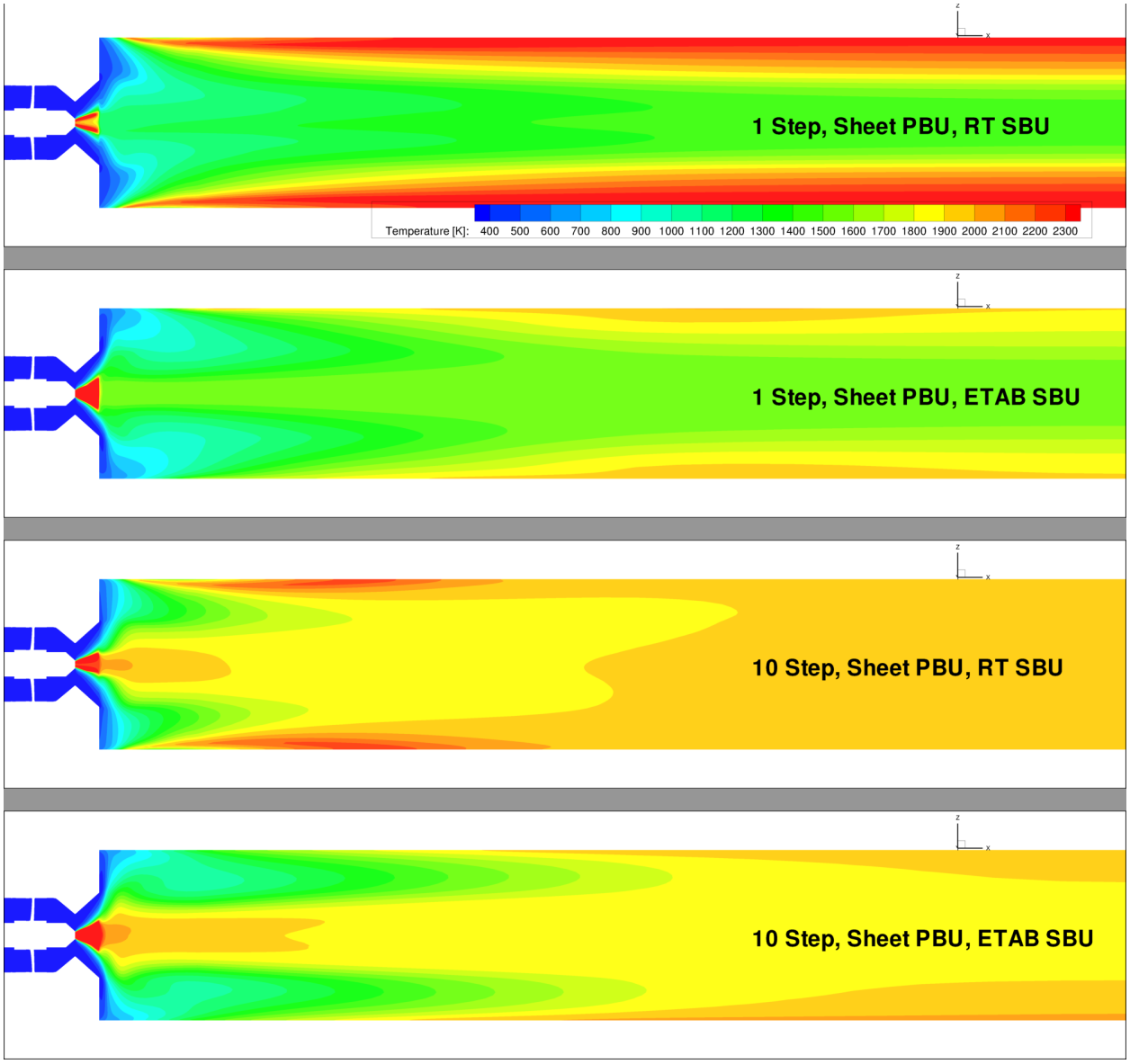

Figure 9.—Contours of temperature [K] using single step and ten step chemistry with the sheet model for primary break-up and various secondary break-up models at the Y = 0 mm mid-plane.

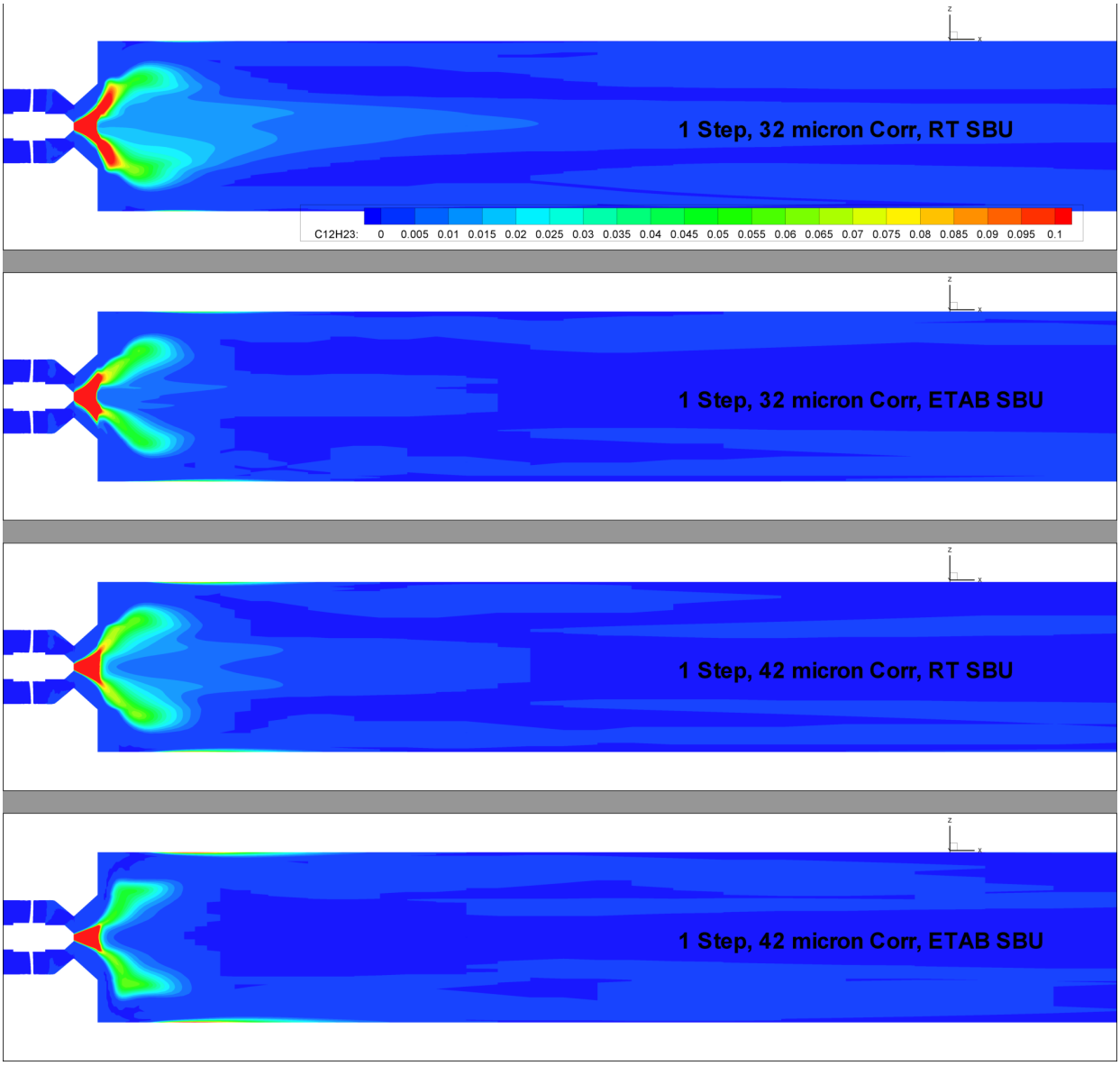

Figure 10.—Contours of fuel mass fraction (Jet-A, $C_{12}H_{23}$) using single step chemistry with the atomization correlation for primary break-up and various secondary break-up models at the Y = 0 mm mid-plane.

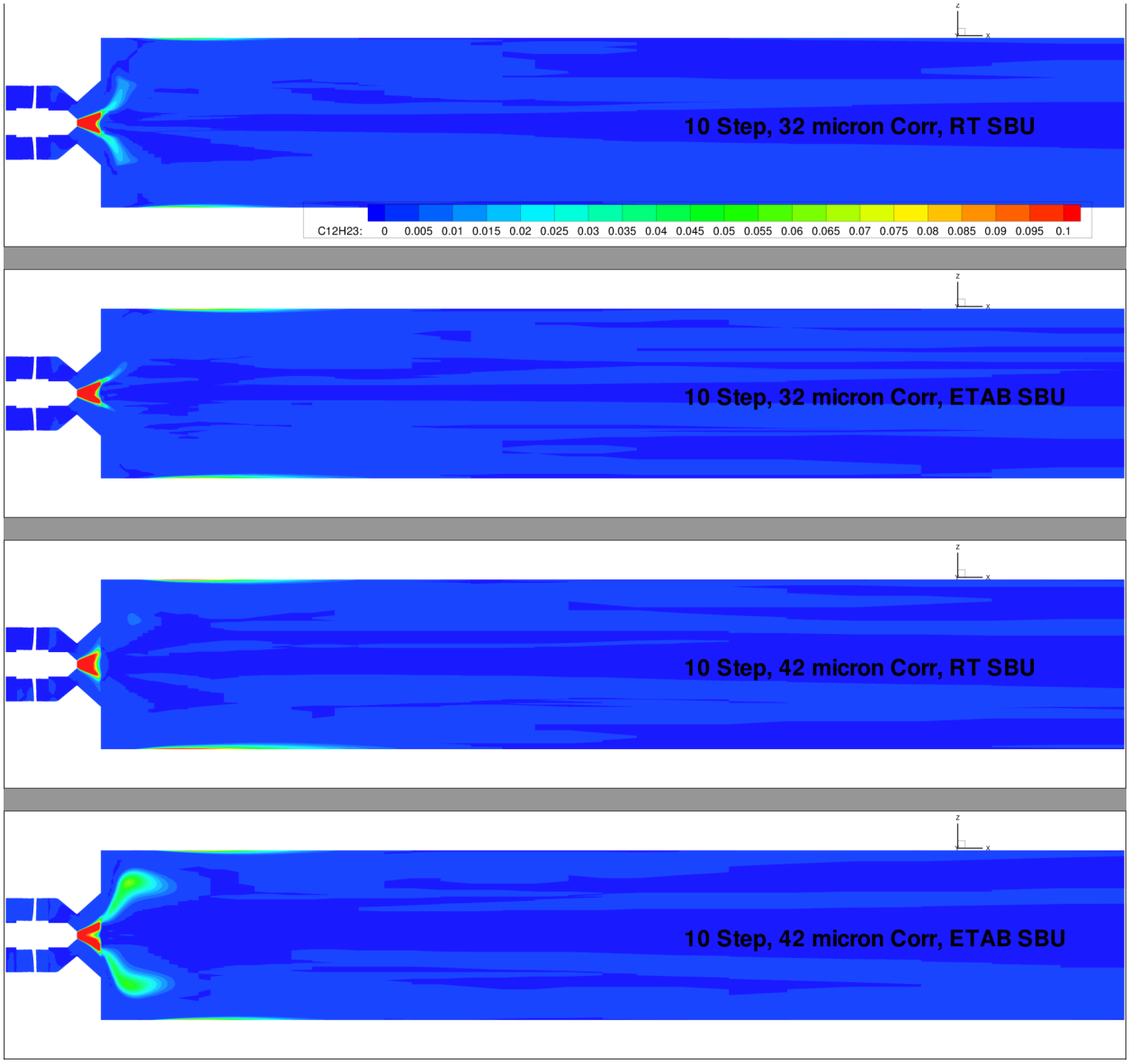

Figure 11.—Contours of fuel mass fraction (Jet-A, $C_{12}H_{23}$) using ten step chemistry with the atomization correlation for primary break-up and various secondary break-up models at the Y = 0 mm mid-plane.

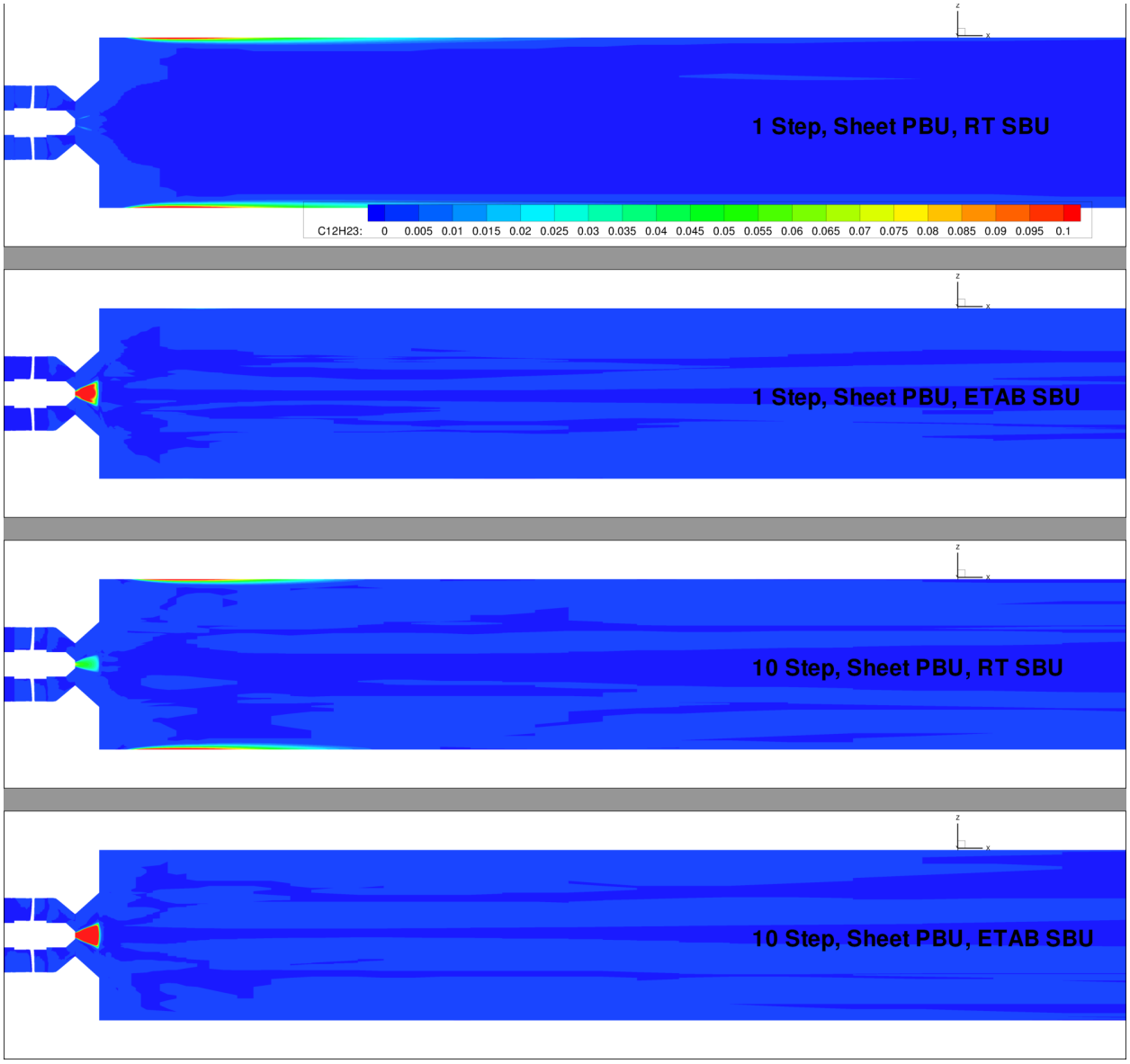

Figure 12.—Contours of fuel mass fraction (Jet-A, $C_{12}H_{23}$) using single step and ten step chemistry with the sheet model for primary break-up and various secondary break-up models at the Y = 0 mm mid-plane.

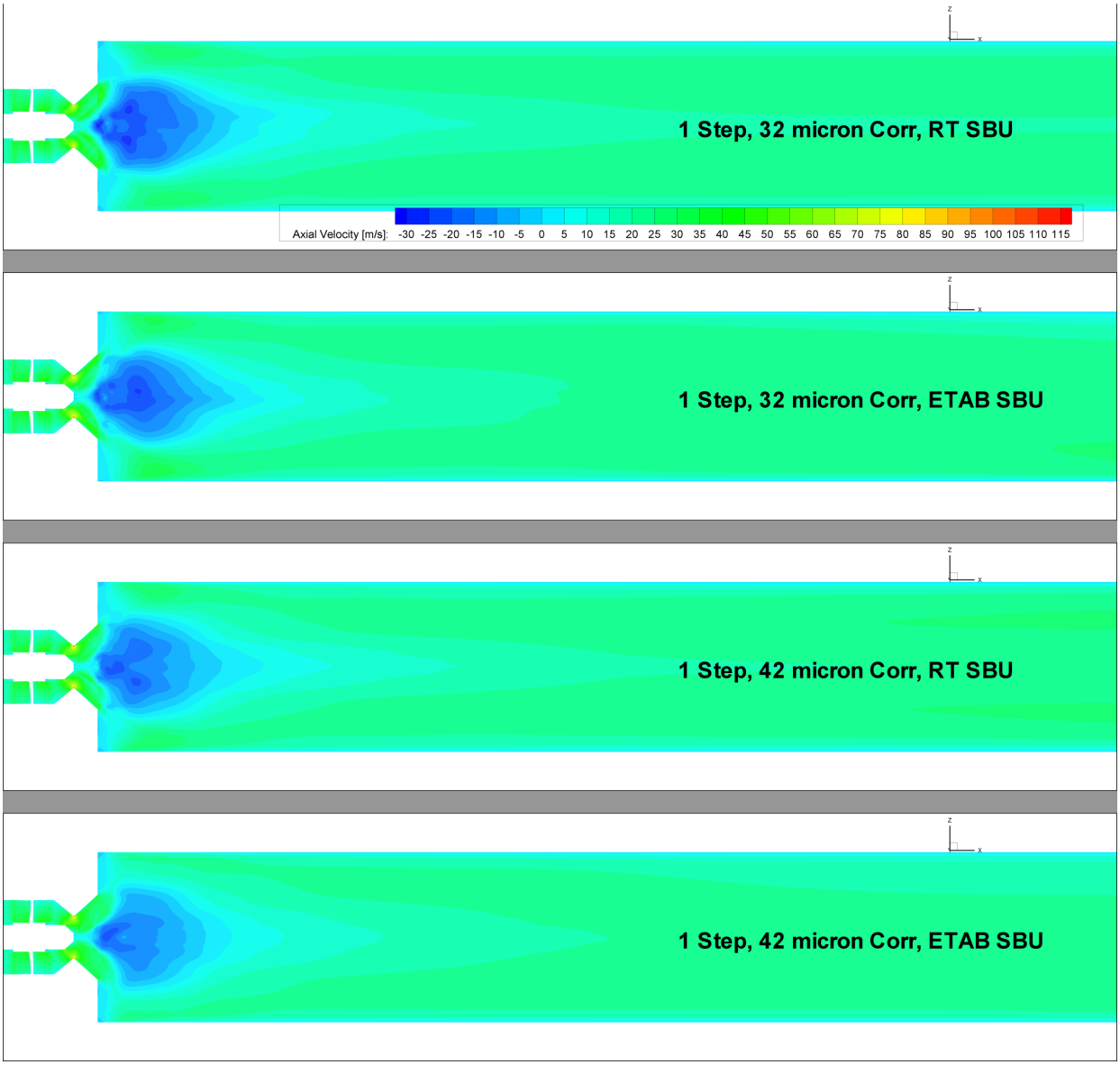

Figure 13.—Contours of axial velocity [m/s] using single step chemistry with the atomization correlation for primary break-up and various secondary break-up models at the Y = 0 mm mid-plane.

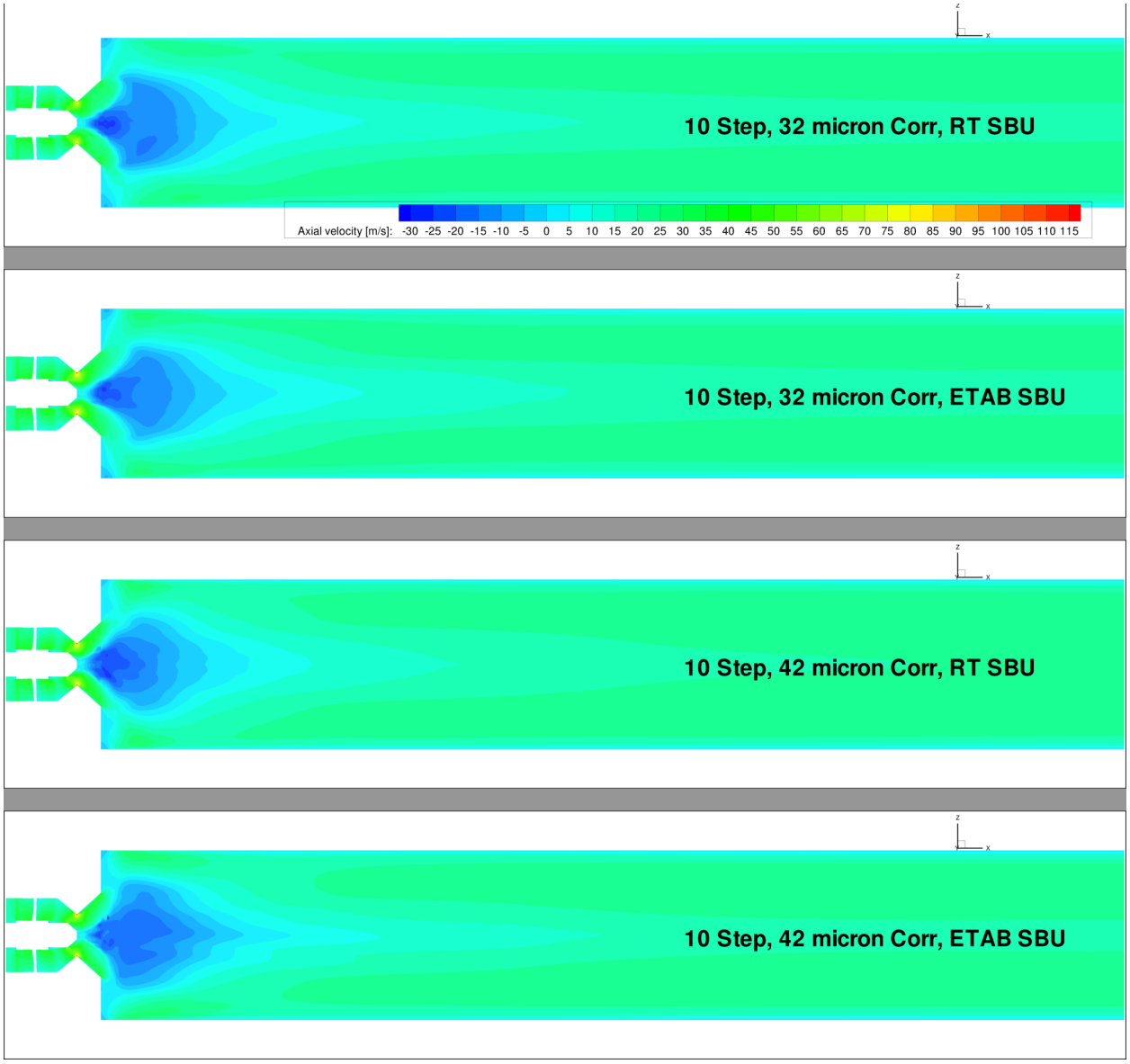

Figure 14.—Contours of axial velocity [m/s] using ten step chemistry with the atomization correlation for primary break-up and various secondary break-up models at the Y = 0 mm mid-plane.

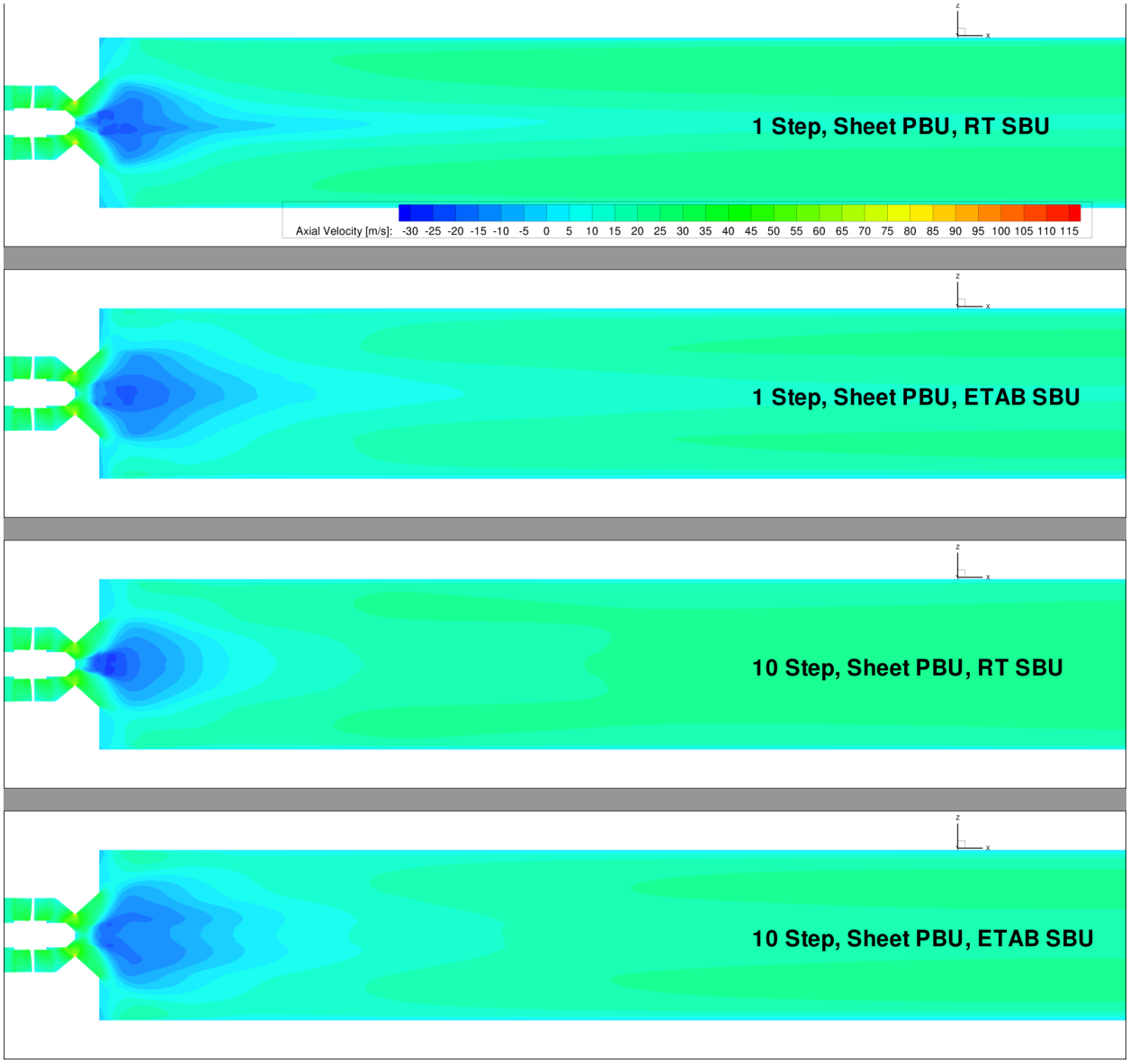

Figure 15.—Contours of axial velocity [m/s] using single step and ten step chemistry with the sheet model for primary break-up and various secondary break-up models at the Y = 0 mm mid-plane.

4.3 Droplet Size Comparison

Figures 16 to 23 compare CFD versus experimental data for the D_{10} droplet size (simple average), while Figures 24 to 31 compare CFD versus experimental data for the D_{32} mean size, the Sauter Mean Diameter (SMD, an approximation of mean droplet surface area). The plots show radial rakes in the X-Z mid-plane (experimental coordinates) at 3, 5, 7, 9, 12, 15, 20, and 25 mm downstream from the injector face (approximately 7 mm from the injector tip, which is located at the narrowest portion of the swirler venturi).

Figures 16 and 17 show a good comparison for the correlation versus experimental data, except for the sheet break-up model, which shows a droplet size over-prediction by at least a factor of five. Given these results, it is obvious that the sheet break-up model produces droplets that are too large. Staying with the correlation (both droplet sizes) we basically observe a decrease in the center instead of a peak. However, this difference is fairly small. The CFD shows no droplets in the center starting at 9 mm downstream of the injector face. This gap becomes more pronounces and the rakes move toward 25 mm. Experimental data set one does not show this gap, and is surprisingly even at an approximately constant 50 μm. Experimental data set two does not show any droplets in the center, starting a 20 mm from the injector face.

Looking at the D_{32}, Figure 25 shows that the correlation produces fairly constant droplet size, with a slight decrease in the center, while the experimental data produces a local minimum at the center, with two symmetrically peaks moving radially outward ("a volcano"). The correlation under-predicts the SMD by a factor of two, while the sheet break-up model over-predicts by a factor of two and a half. As we move downstream, generally the comparison improves, but we see that using the correlation, we get a minimum for the CFD droplet size in the radial center versus a peak shown by the experimental data. Figure 26 surprisingly shows a good comparison for the sheet break-up model using the RT secondary atomization model. As with the D_{10} droplet size, the D_{32} CFD results show no droplets in the center beginning at 9 mm from the injector face. Qualitatively, the correlation at least has a similar shape as the experimental data. 20 mm downstream (Fig. 30), the correlation compares well with the second set of experimental data.

Given both the D_{10} and D_{32} droplet sizes, it seems that the use of the given correlation for primary atomization gives better results. At this time, we cannot conclude with secondary atomization model is more accurate, because they appear to be producing similar results.

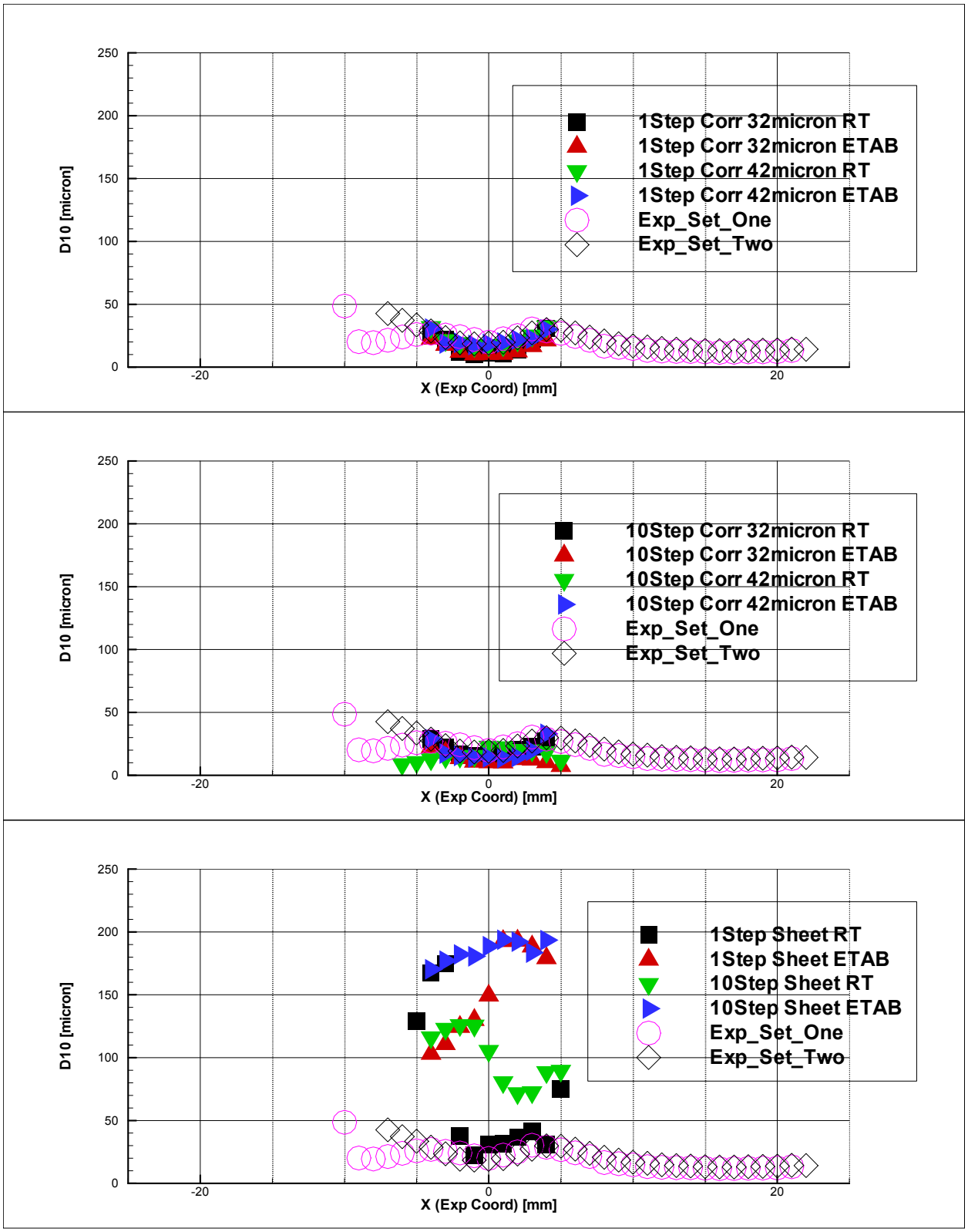

Figure 16.—Line Plots of D_{10} [microns] versus the radial axis X [mm], in the experimental coordinate frame, for CFD and experimental data 3 mm downstream of the injector face in the X-Z mid-plane.

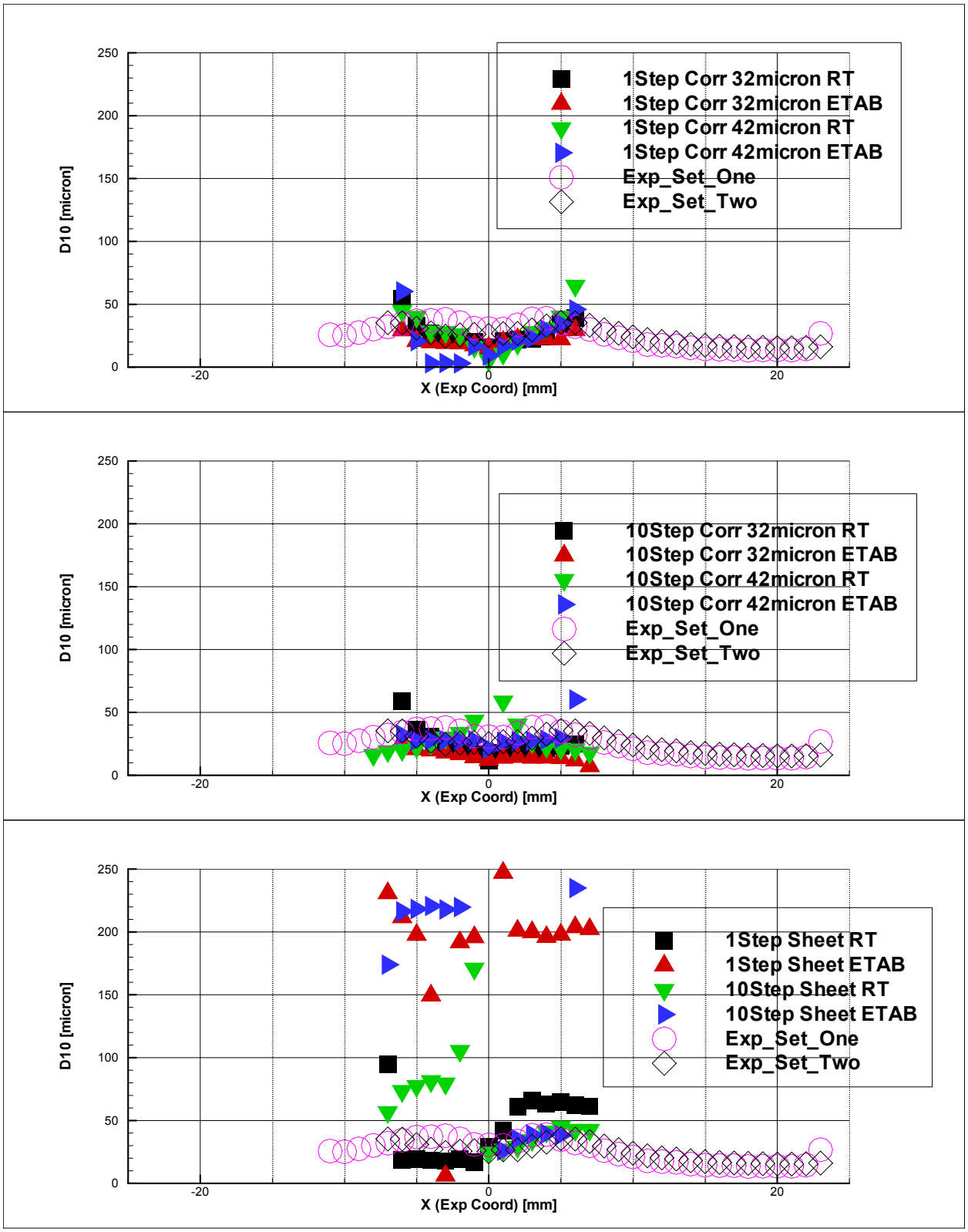

Figure 17.—Line Plots of D_{10} [microns] versus the radial axis X [mm], in the experimental coordinate frame, for CFD and experimental data 5 mm downstream of the injector face in the X-Z mid-plane.

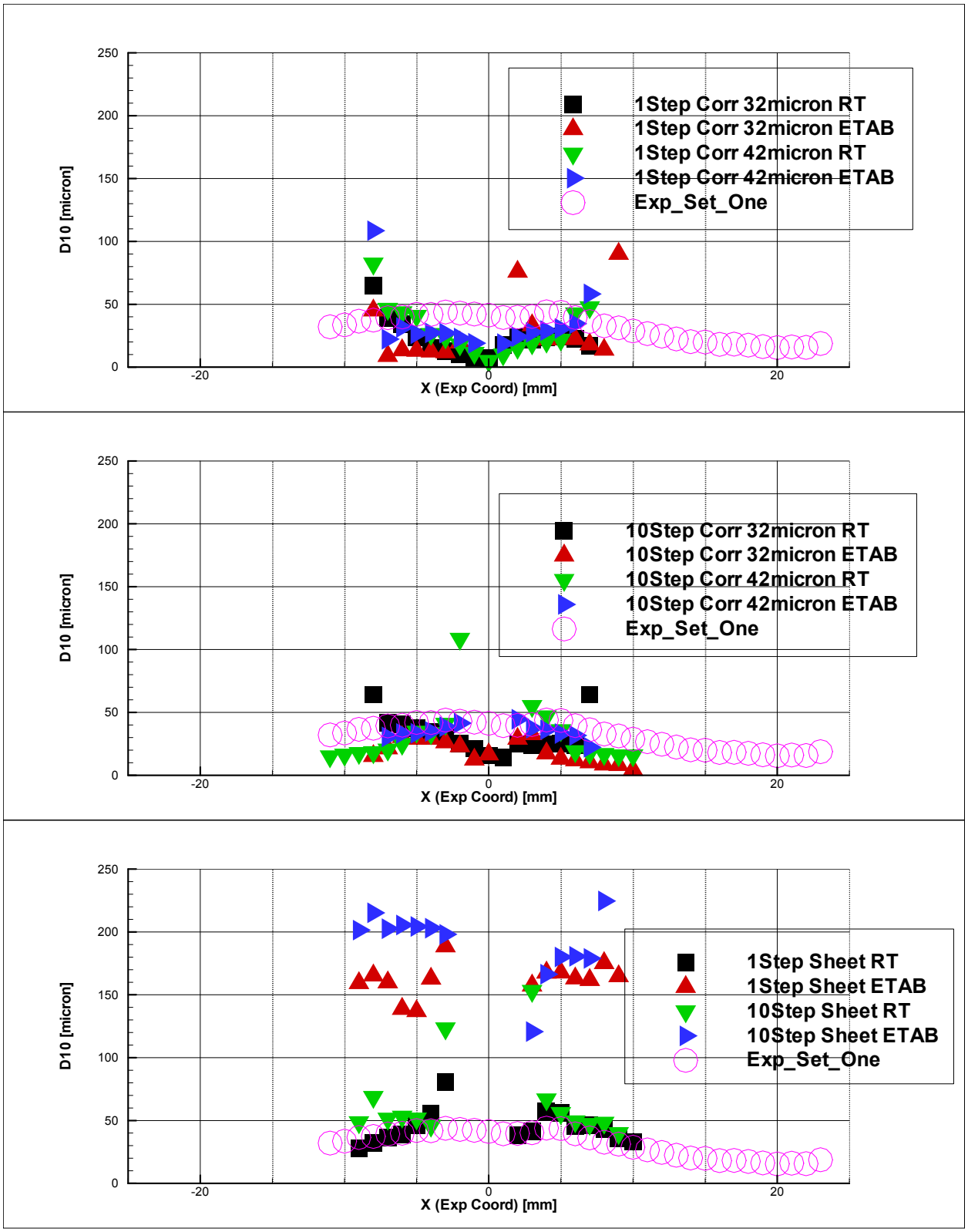

Figure 18.—Line Plots of D_{10} [microns] versus the radial axis X [mm], in the experimental coordinate frame, for CFD and experimental data 7 mm downstream of the injector face in the X-Z mid-plane.

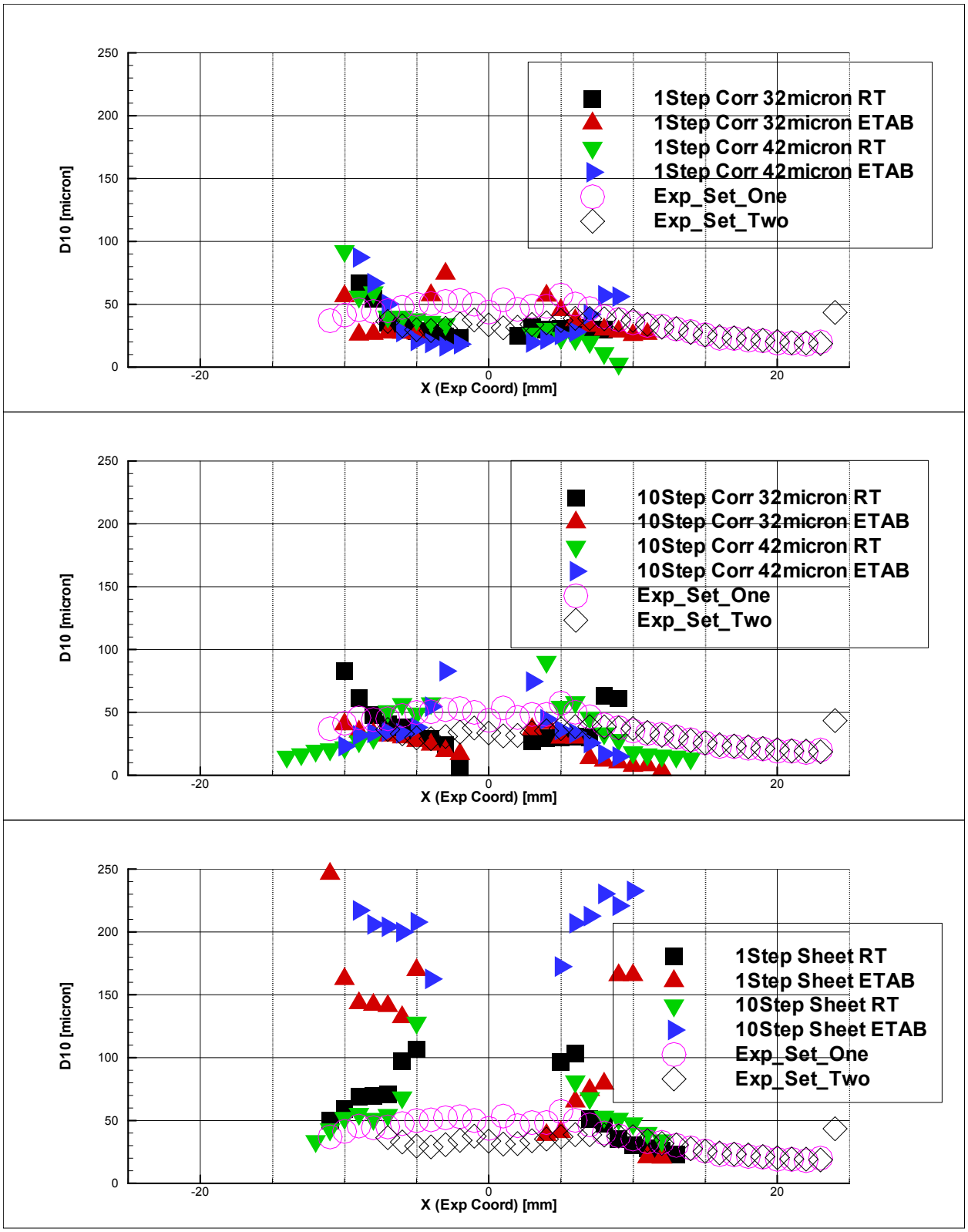

Figure 19.—Line Plots of D_{10} [microns] versus the radial axis X [mm], in the experimental coordinate frame, for CFD and experimental data 9 mm downstream of the injector face in the X-Z mid-plane.

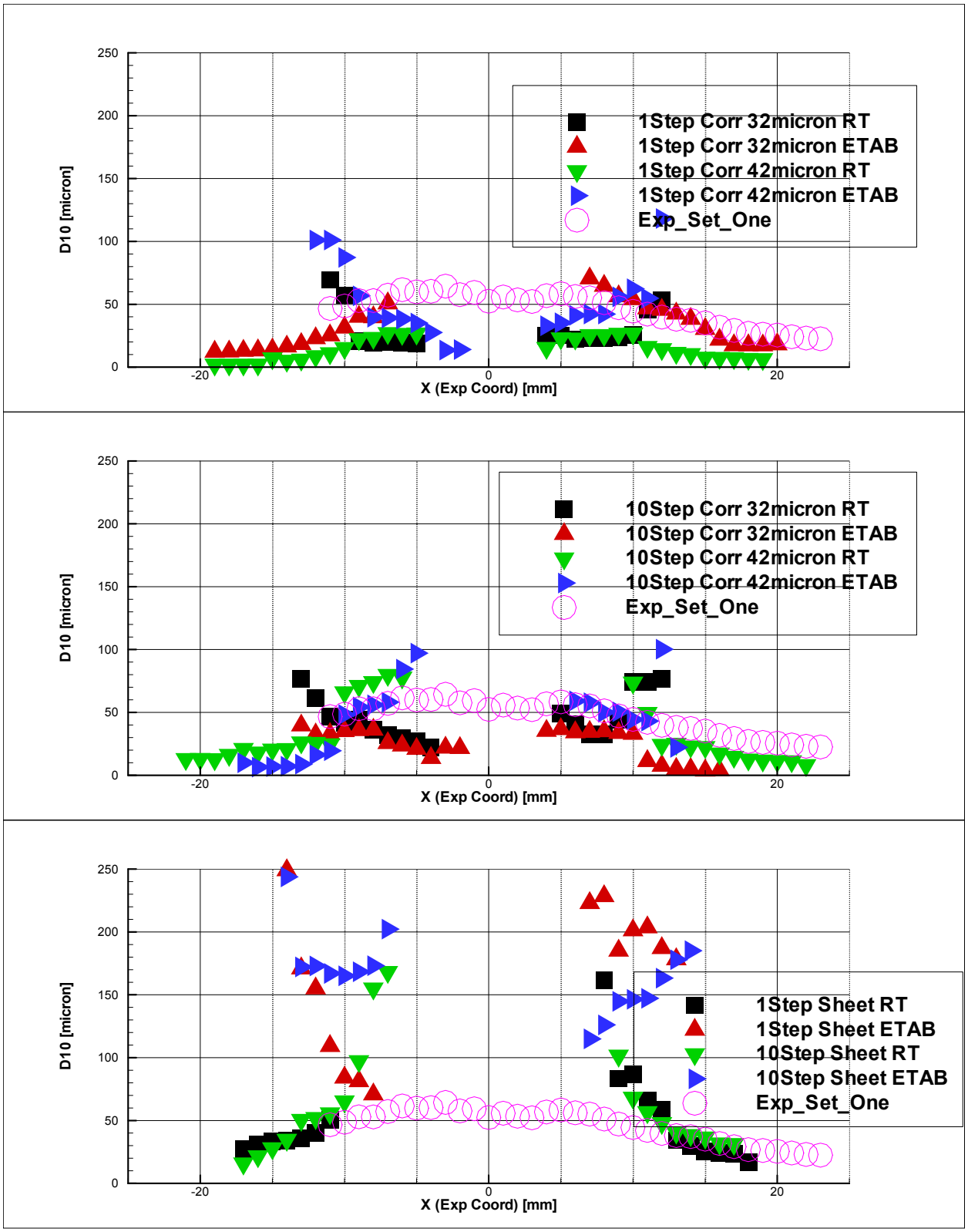

Figure 20.—Line Plots of D_{10} [microns] versus the radial axis X [mm], in the experimental coordinate frame, for CFD and experimental data 12 mm downstream of the injector face in the X-Z mid-plane.

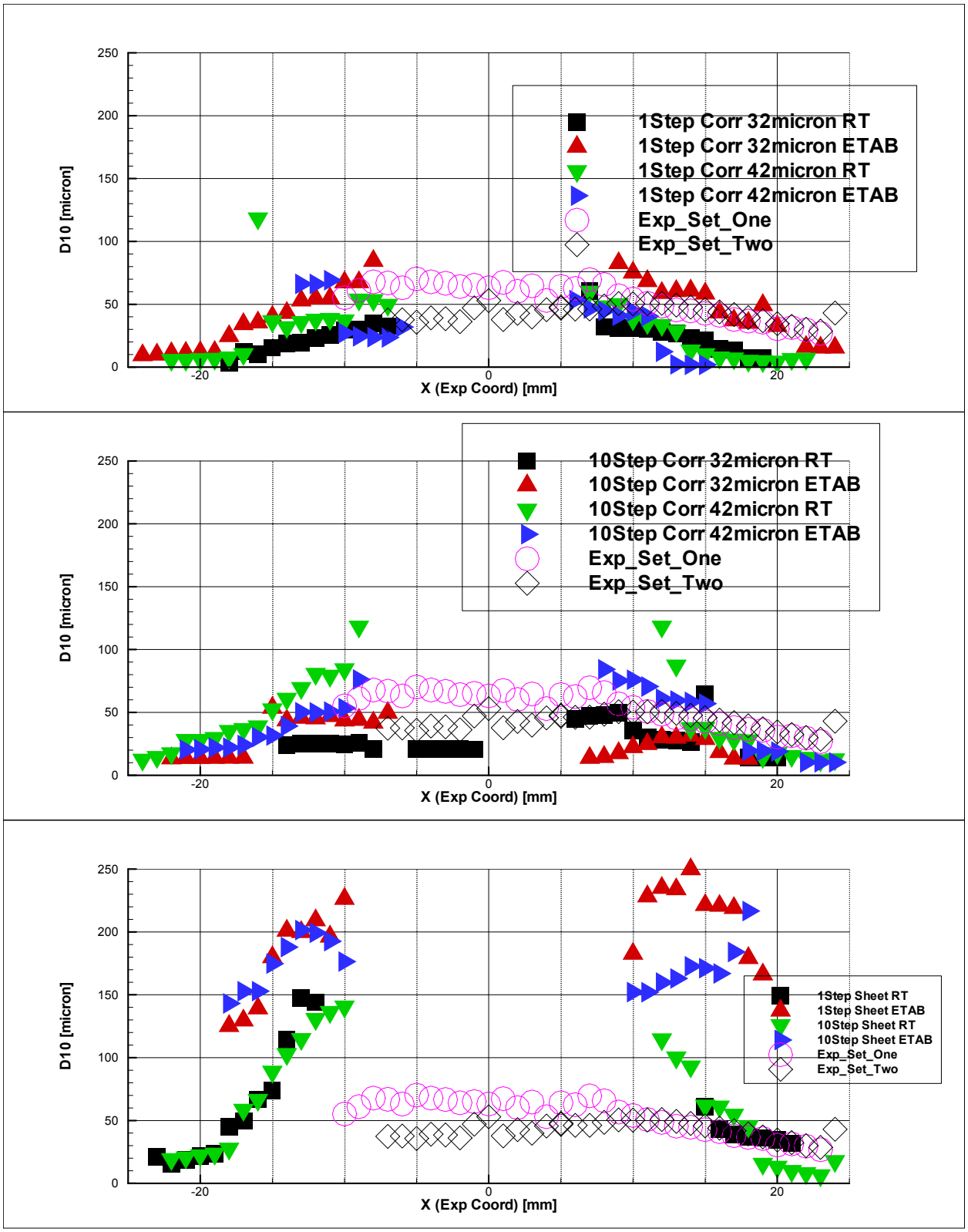

Figure 21.—Line Plots of D_{10} [microns] versus the radial axis X [mm], in the experimental coordinate frame, for CFD and experimental data 15 mm downstream of the injector face in the X-Z mid-plane.

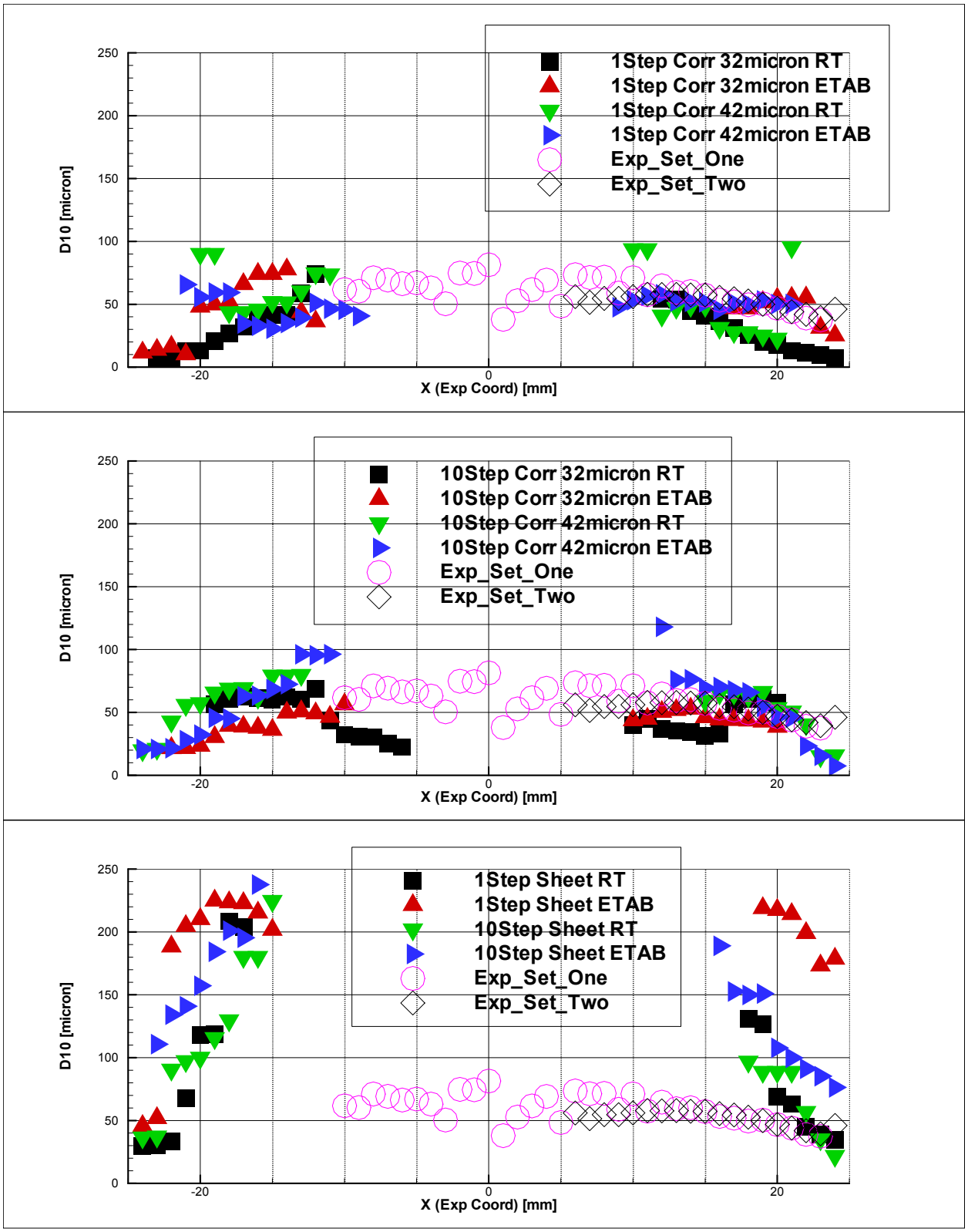

Figure 22.—Line Plots of D_{10} [microns] versus the radial axis X [mm], in the experimental coordinate frame, for CFD and experimental data 20 mm downstream of the injector face in the X-Z mid-plane.

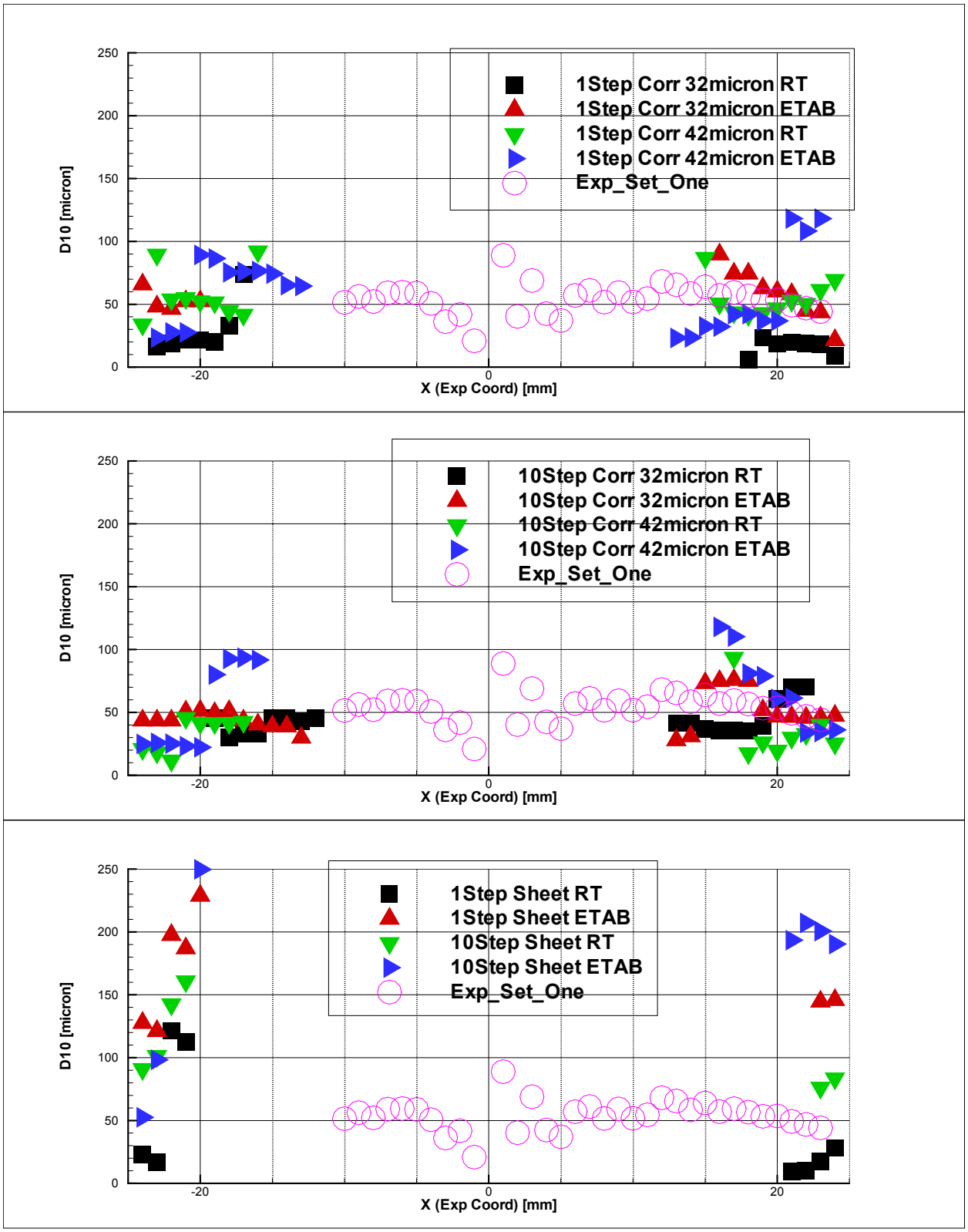

Figure 23.—Line Plots of D_{10} [microns] versus the radial axis X [mm], in the experimental coordinate frame, for CFD and experimental data 25 mm downstream of the injector face in the X-Z mid-plane.

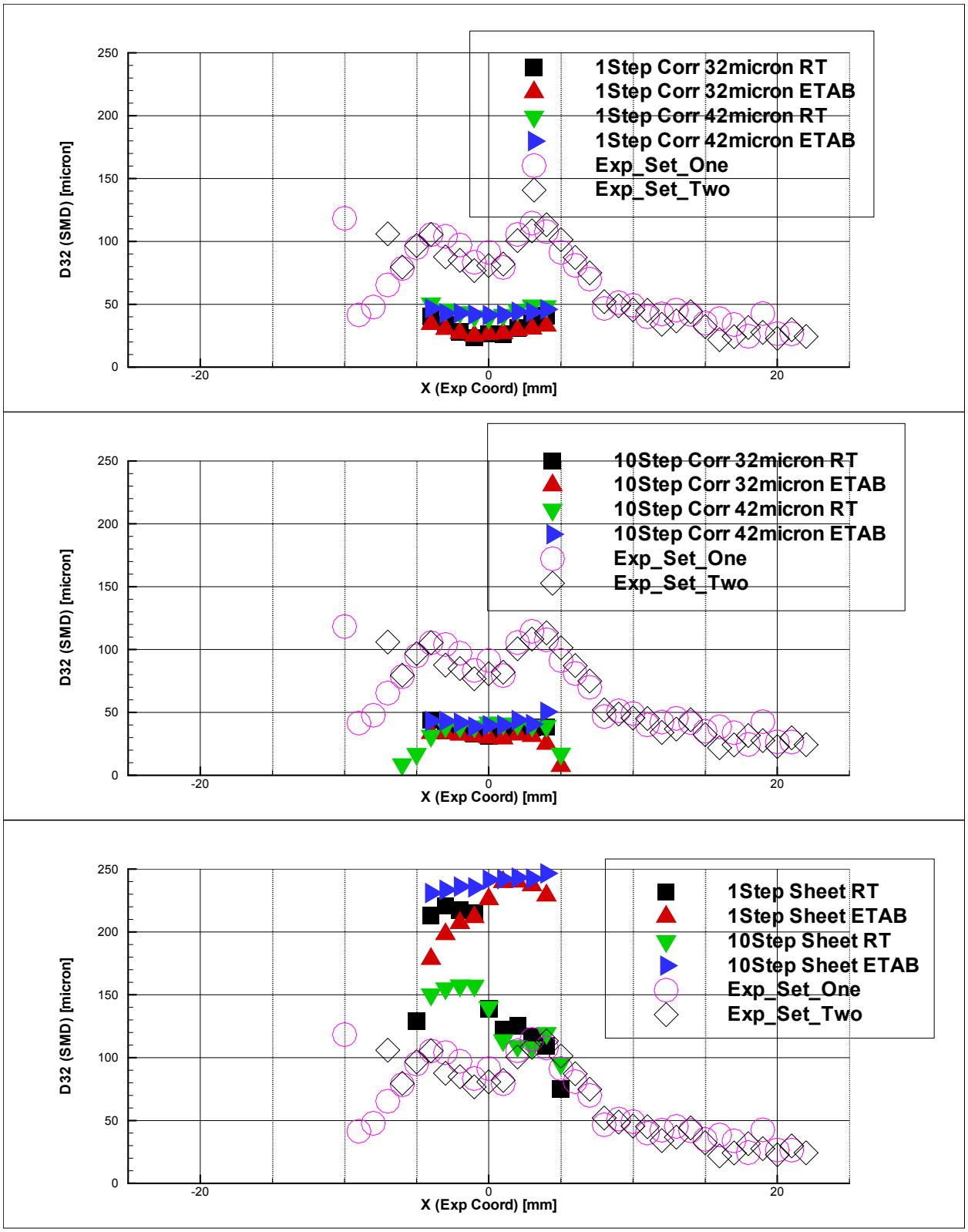

Figure 24.—Line Plots of D_{32} [microns] versus the radial axis X [mm], in the experimental coordinate frame, for CFD and experimental data 3 mm downstream of the injector face in the X-Z mid-plane.

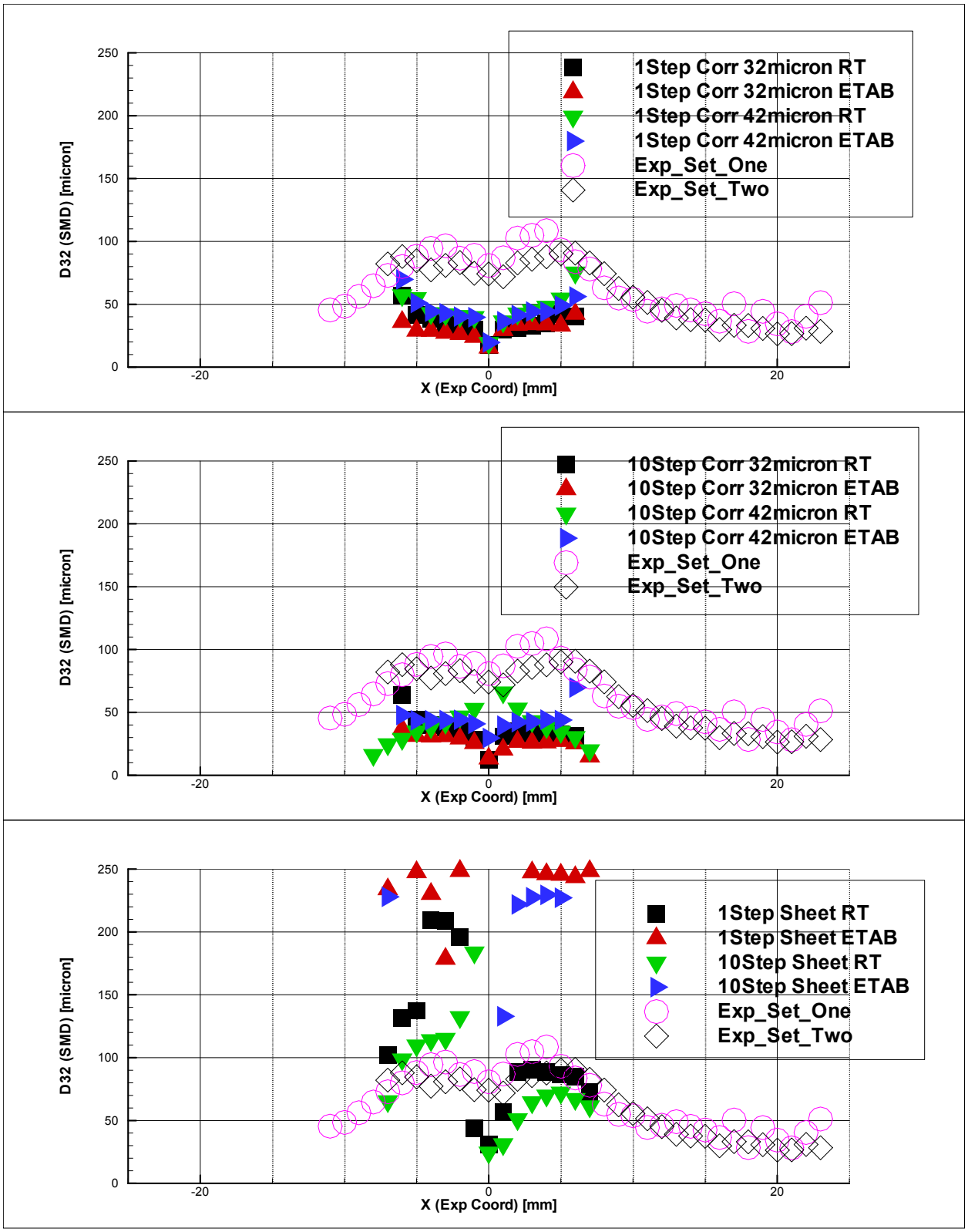

Figure 25.—Line Plots of D_{32} [microns] versus the radial axis X [mm], in the experimental coordinate frame, for CFD and experimental data 5 mm downstream of the injector face in the X-Z mid-plane.

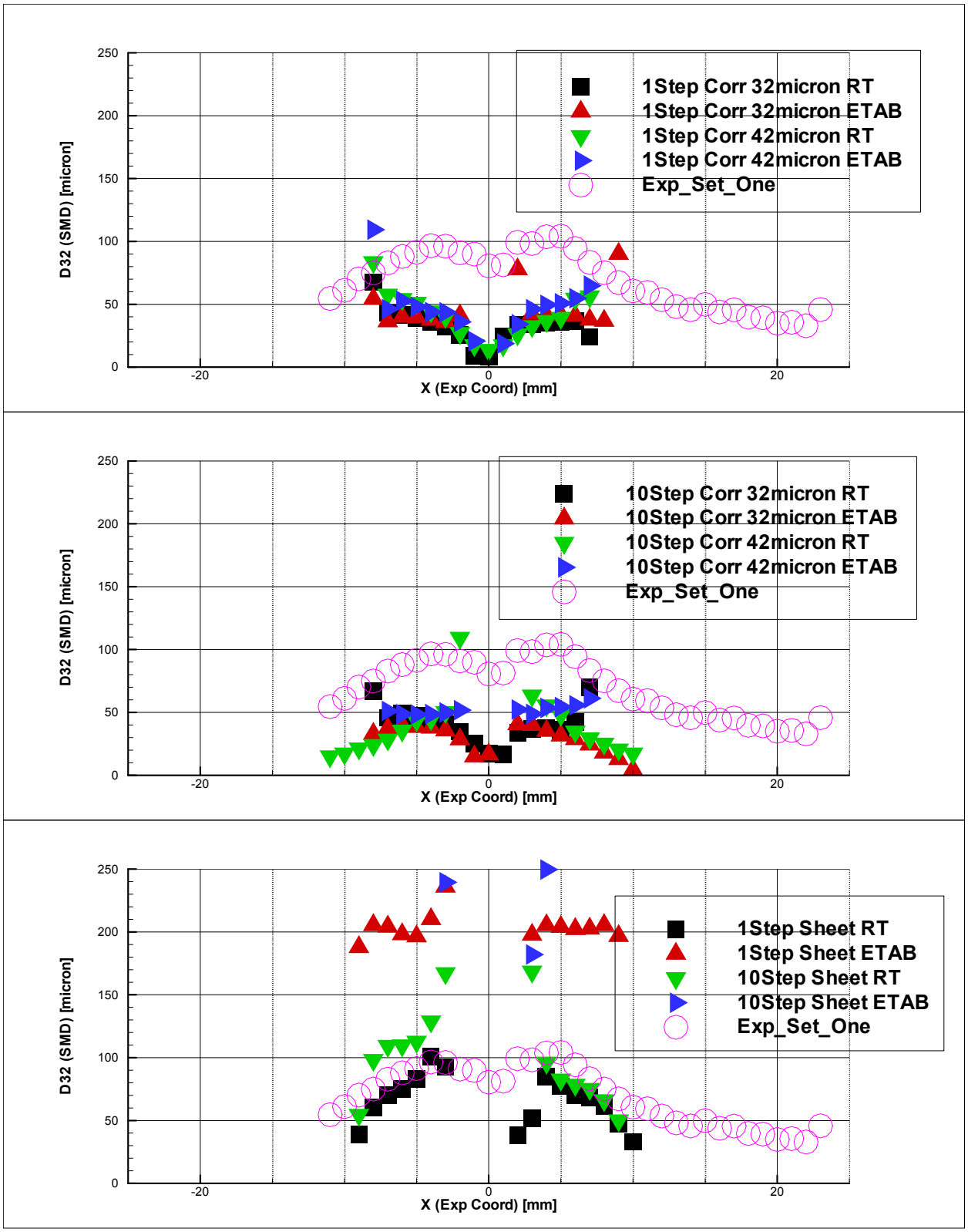

Figure 26.—Line Plots of D_{32} [microns] versus the radial axis X [mm], in the experimental coordinate frame, for CFD and experimental data 7 mm downstream of the injector face in the X-Z mid-plane.

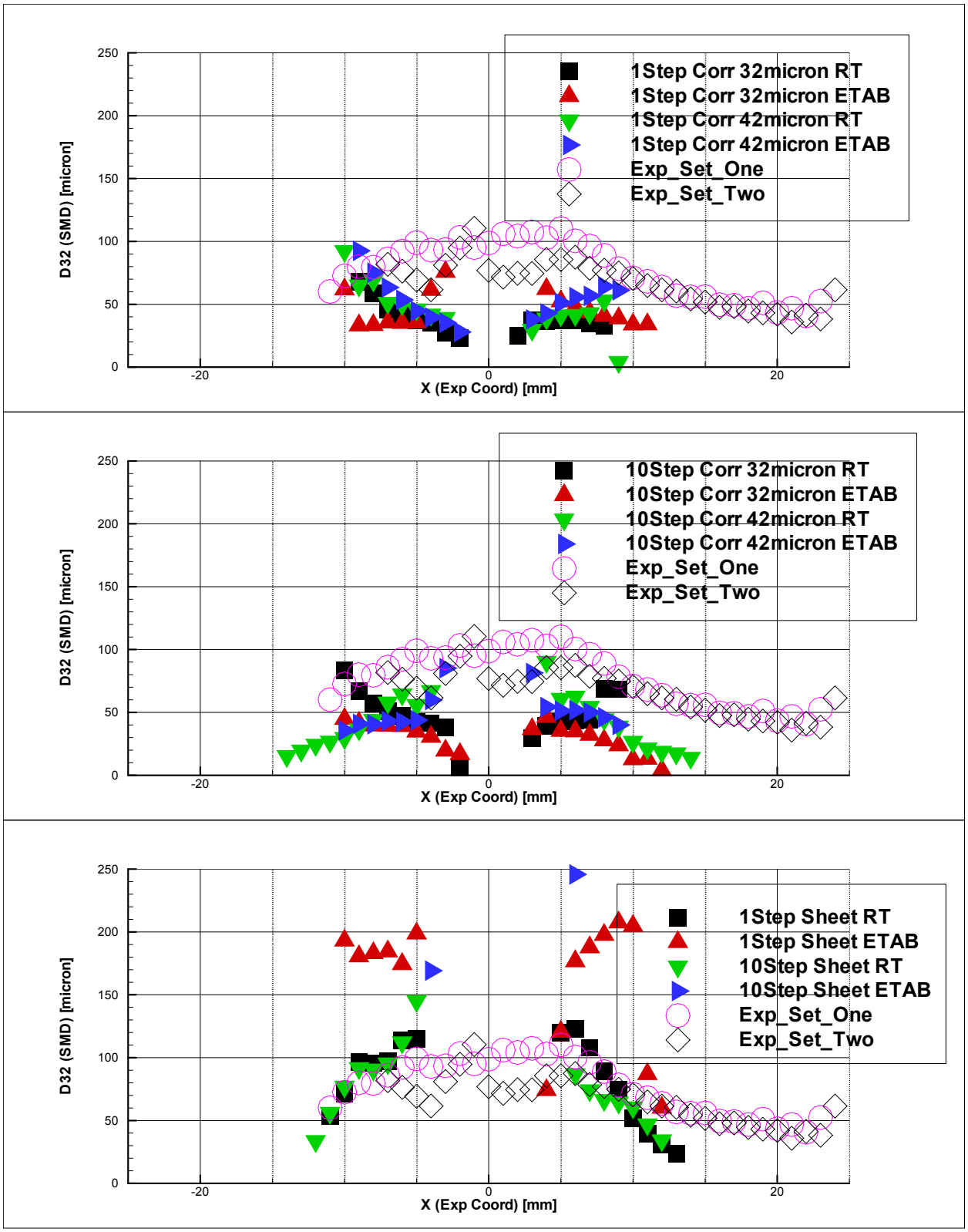

Figure 27.—Line Plots of D_{32} [microns] versus the radial axis X [mm], in the experimental coordinate frame, for CFD and experimental data 9 mm downstream of the injector face in the X-Z mid-plane.

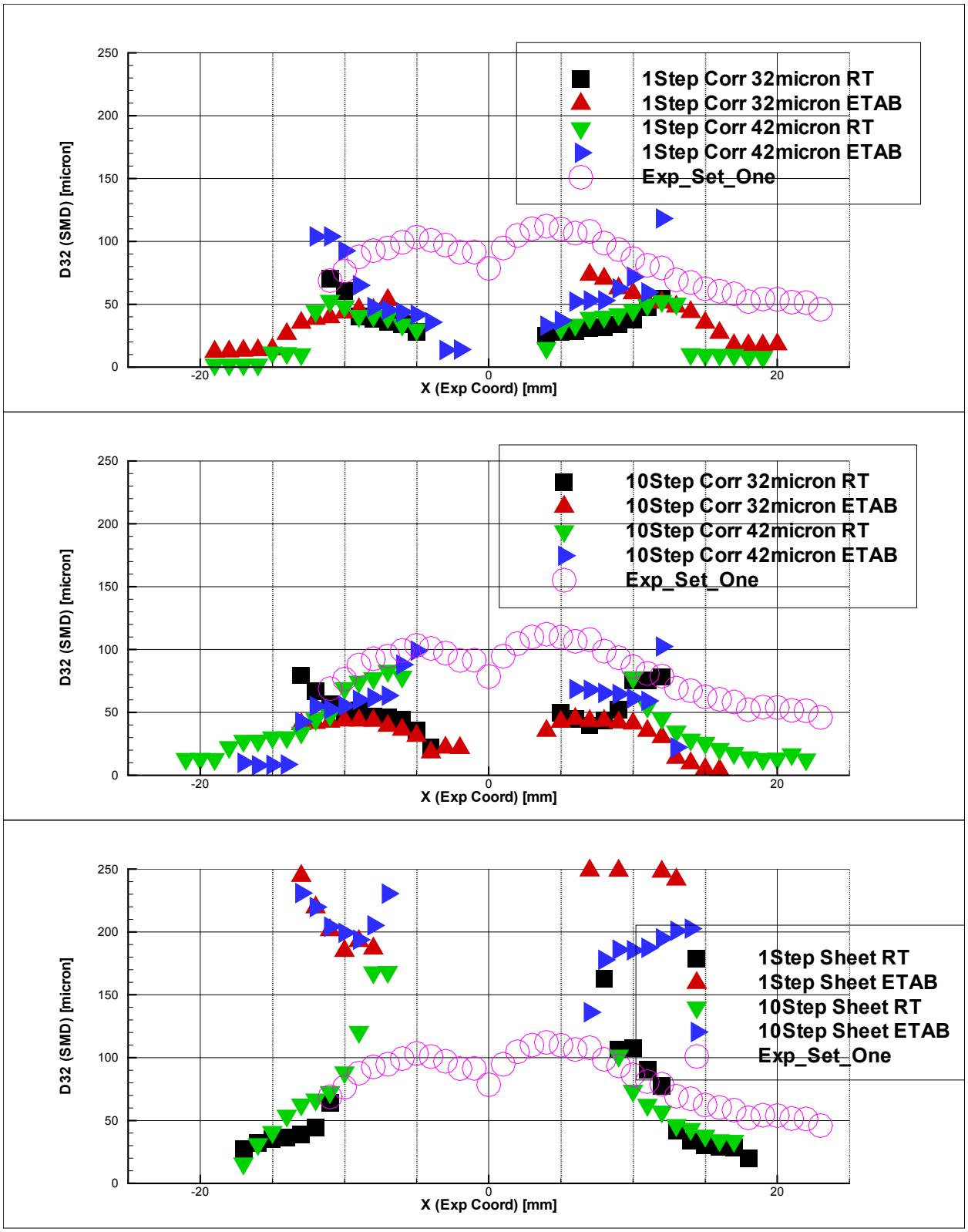

Figure 28.—Line Plots of D_{32} [microns] versus the radial axis X [mm], in the experimental coordinate frame, for CFD and experimental data 12 mm downstream of the injector face in the X-Z mid-plane.

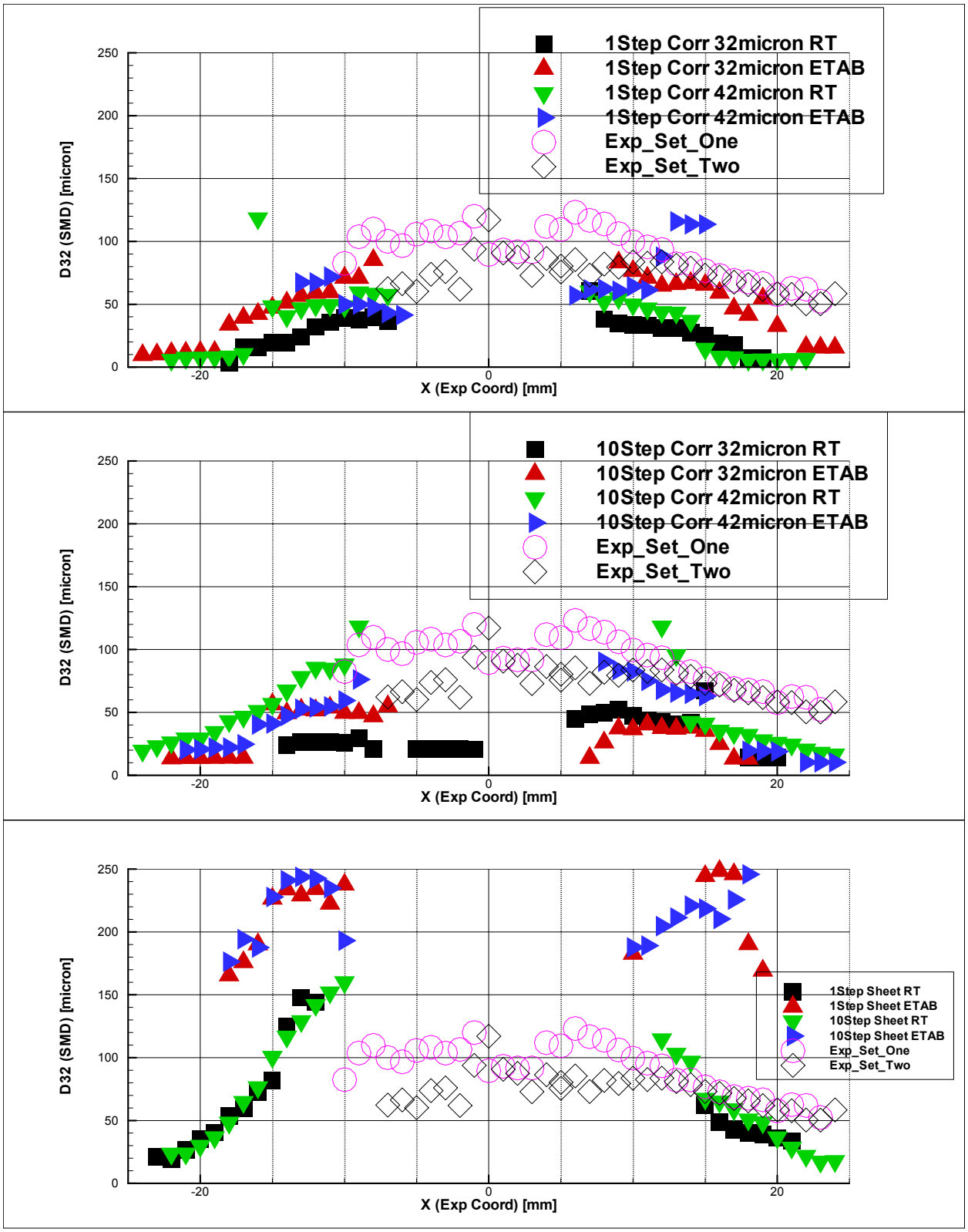

Figure 29.—Line Plots of D_{32} [microns] versus the radial axis X [mm], in the experimental coordinate frame, for CFD and experimental data 15 mm downstream of the injector face in the X-Z mid-plane.

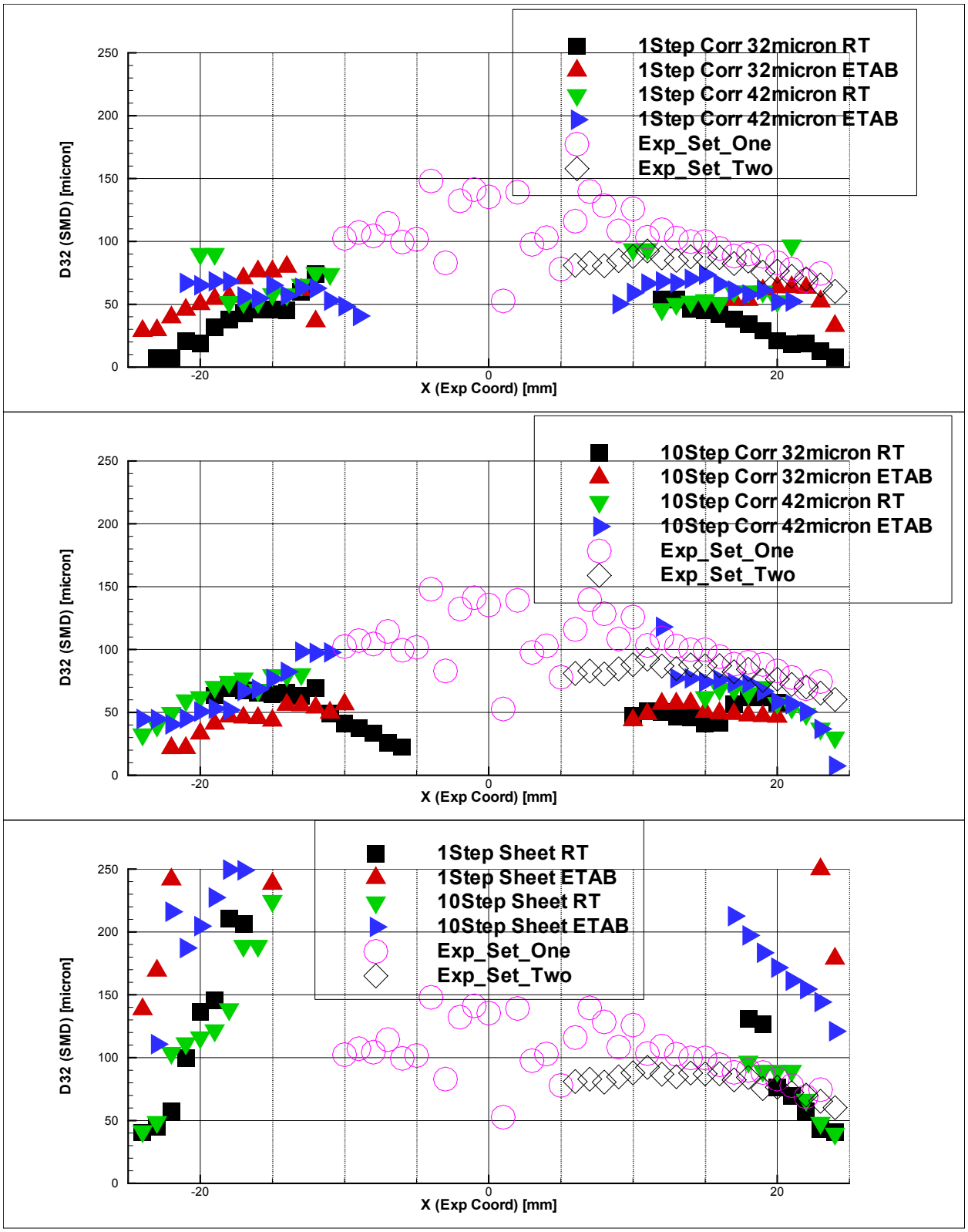

Figure 30.—Line Plots of D_{32} [microns] versus the radial axis X [mm], in the experimental coordinate frame, for CFD and experimental data 20 mm downstream of the injector face in the X-Z mid-plane.

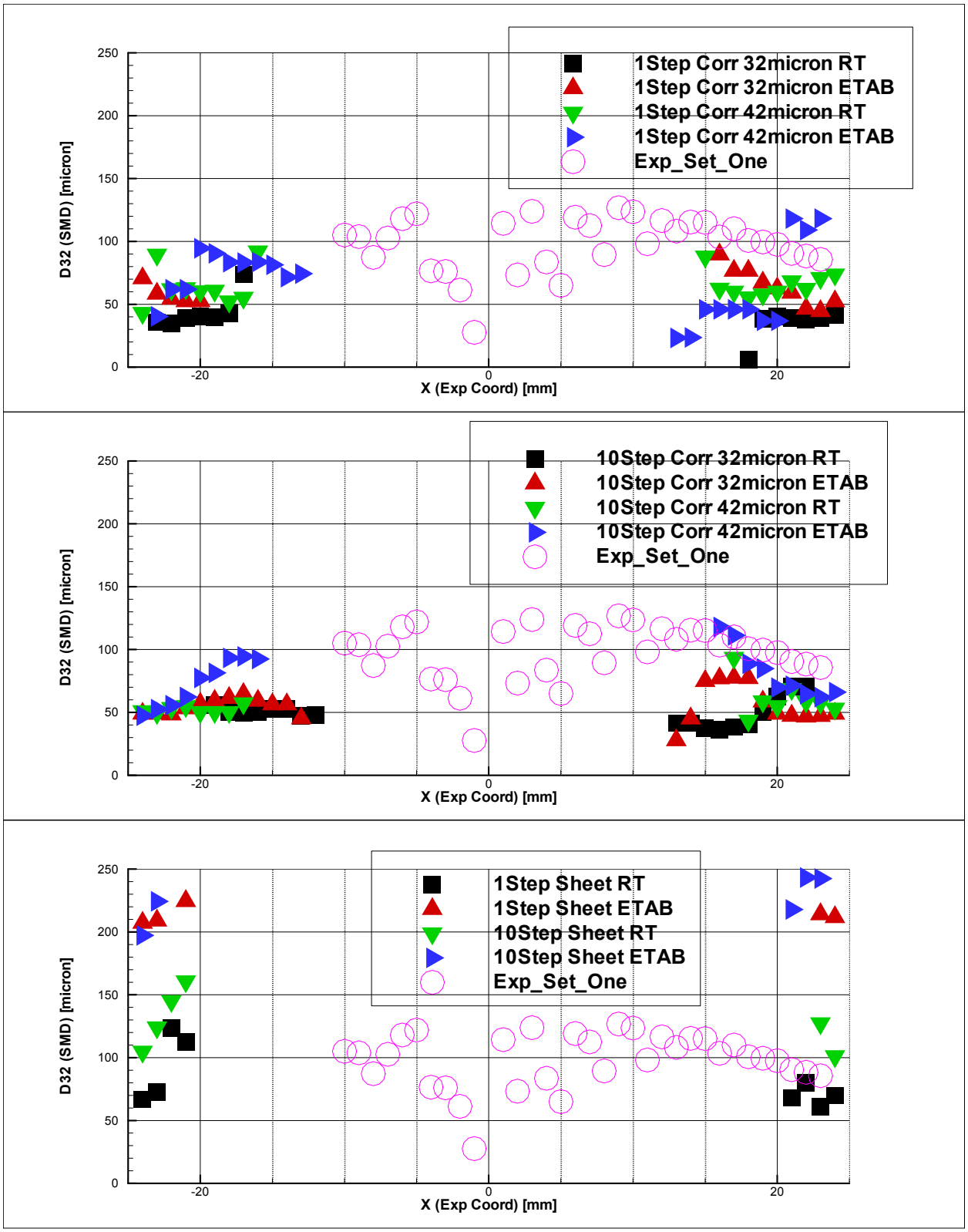

Figure 31.—Line Plots of D_{32} [microns] versus the radial axis X [mm], in the experimental coordinate frame, for CFD and experimental data 25 mm downstream of the injector face in the X-Z mid-plane.

4.4 Major Differences Between Steady-State RANS and Transient Flow Studies

Results from PRNS simulations at NASA Glenn Research Center, and LES flow simulations from Stanford and Georgia Tech have shown that a strong vortex core influences the flow field near the LDI fuel injector tip. Figure 32 shows the vortex core and unsteady streak lines from a PRNS simulation. This vortex is an unsteady flow feature and its mean cannot be approximate through current turbulence modeling techniques and will probably never be modeled, the resolution of this flow feature will always have to have some "directly resolved technique." It is believed that this flow feature enhances dispersion the spray droplets, and greatly improves the emission reduction performance of this LDI fuel injector. Therefore, we believe future single swirler LDI simulations should always be PRNS or LES transient flow simulations to accurately compute injector/combustor performance.

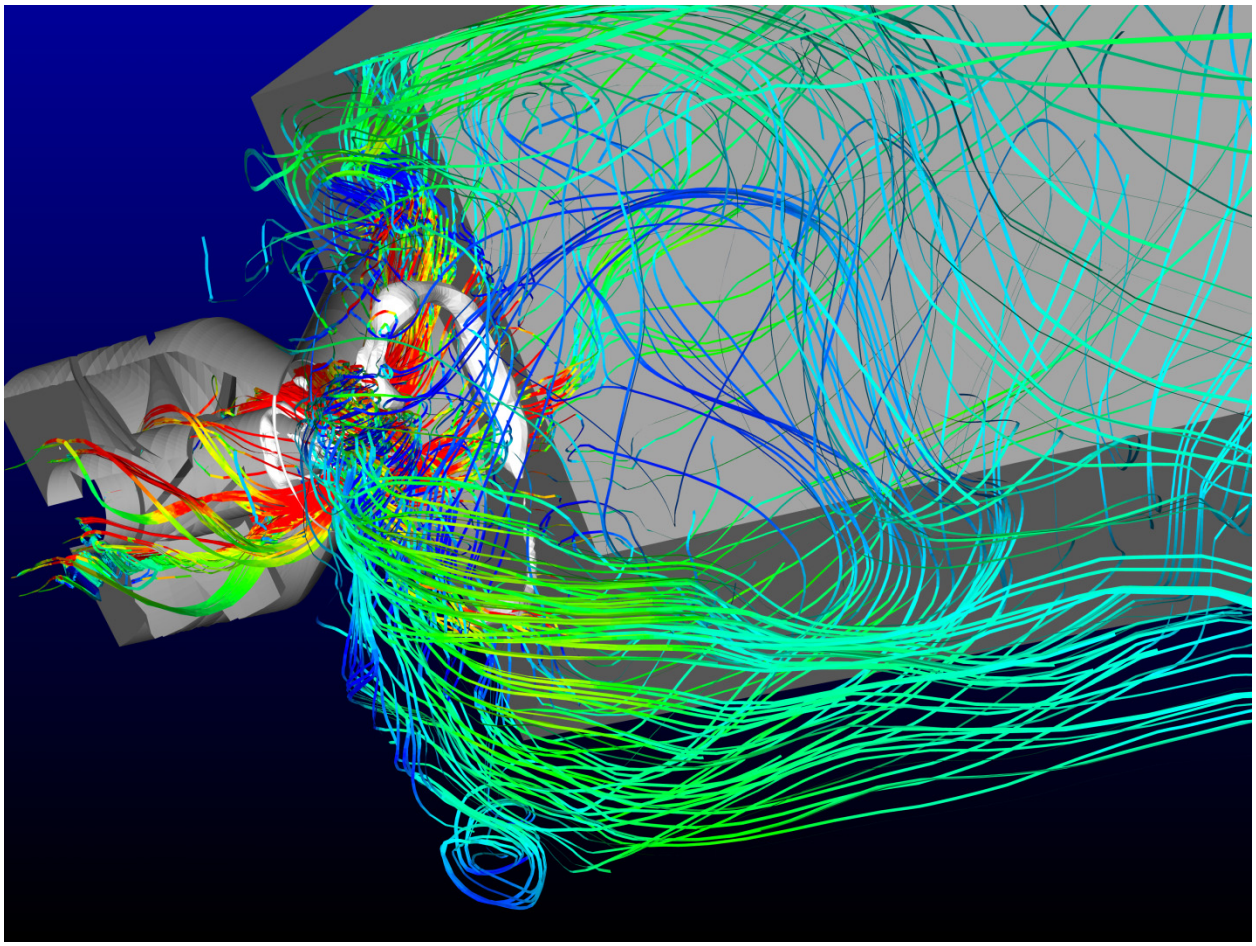

Figure 32.—A PRNS mixing study of a Lean Direct Injection (LDI) combustor swirler. Pathlines are colored by axial velocity. The white isosurface of pressure elucidates the vortex core resulting from the swirler. (Courtesy: J. Horowitz).

4.4.1 Weaknesses of Both the Correlation and Primary Break-Up Modeling Approach

The use of correlations, even for a specific fuel injector for LDI combustor, is that the flow field *cannot be decoupled* from the atomization process. Without out a standalone fuel injector, spray droplet measurements usually cannot be accurately measured; including the venturi in most LDI designs usually does not allow optical access for PDPA measurement. Also, as shown by numerous CFD results (including this one), combustion occurs in the primary atomization area, which is another coupling process.

The problem with using break-up models is that at some point, they use correlated film thickness data from Lefebvre, and assume some type of distribution shape. In this paper, based on the spray size comparison, it appears that the χ^2 statistical correlation in the current implementation of the LISA model is not a valid assumption. Rosin-Rammler, the distribution used in the correlation, should be tried instead.

We believe the film thickness, at the very least, must be directly computed. If possible, the atomization process should be directly simulated with combustion; perhaps up to 3 mm downstream of the fuel injector tip, and then continue the calculation with lagrangian dilute spray modeling.

5.0 Conclusions

We have thoroughly explored the single swirler LDI validation case with a variety of primary and secondary break-up atomization models. Comparisons against experimental data show that the use of the correlation for primary spray break-up implemented by Raju in the NCC produces most realistic results, but this result needs to be improved. Given the single or ten step chemical kinetics models, use of a spray size correlation gives similar, acceptable results. For current LDI simulations, a spray size correlation should be used over the current sheet break-up model. We believe this case needs to be further explored by directly calculating the film thickness of the pressure swirl atomizer used in the single swirler LDI case, and the use of LES as a flow solution method.

References

1. Tacina, R., Mansour, A., Partelow, L., Wey, C., "Experimental Sector and Flame-Tube Evaluations of a Multipoint Integrated Module Concept for Low Emission Combustors," GT–2004–53263, ASME Turbo Expo 2004, Vienna, Austria, 2004.
2. Tacina, R., Wey, C., Laing, P., and Mansour, A., "Sector Tests of a Low-NOx, Lean-Direct-Injection, MultiPoint Integrated Module Combustor Concept," GT–2002–30089, 2002.
3. Tacina, R., Wey, C., Laing, P., and Mansour, A., "A Low NOx Lean-Direct Injection, MultiPoint Integrated Module Combustor Concept for Advanced Aircraft Gas Turbines," NASA/TM—2002-211347, Porto, Portugal, July 9–12, 2001.
4. El-Asrag H., and Pitsch H., "Radiation-spray Coupling for Realistic Flow Configurations," Center for Turbulence Research Annual Research Briefs, Stanford University, Stanford, CA, USA, 2008.
5. Patel, N., Menon, S., "Simulation of Spray–Turbulence–Flame Interactions in a Lean Direct Injection Combustor," Combustion and Flame, vol. 153, pp. 228–257, 2008.
6. Davoudzadeh, F., Liu, N.-S., "Validation of the National Combustion Code (NCC)," Presentation, Ultra-Efficient Engine Technology Program Technical Forum, NASA Glenn Research Center, October 27–29, 2003.
7. Davoudzadeh, F., Liu, N.-S., "Numerical Prediction of Non-Reacting and Reacting Flow in a Model Gas Turbine Combustor," GT–2004–53496, Proceedings of the ASME Turbo Expo, Vienna, Austria, 2004.
8. Iannetti, A.C., Liu, N.-S., Davoudzadeh, F., "The Effect of Spray Initial Condition on Heat Release and Emissions in LDI CFD Calculations," NASA/TM—2008-215422, Glenn Research Center, Cleveland, OH, USA, 2009.

9. Cai, J., S.-M. Jeng, S.-M., "The Structure of a Swirl- Stabilized Reacting Spray Issued from an Axial Swirler," AIAA–2005–1424, 43rd AIAA Aerospace Sciences Meeting & Exhibit, 10–13, Reno, NV, USA, 2005.
10. Fu, Y., Jeng, S.-M., Tacina, R., "Characteristics of the Swirling Flow Generated by an Axial Swirler," Proceedings of GT2005 ASME Turbo Expo 2005: Power for Land, Sea and Air June 005, Reno-Tahoe, Nevada, USA, 2005.
11. Stubbs, R., M., and Liu, N.-S., "Preview of the National Combustion Code," AIAA 97–3114, 33rd AIAA/ASME/SAE/ASEE Joint Propulsion Conference and Exhibit, July 6–9, Seattle, WA, USA, 1997.
12. Quealy, A., Ryder, R., Norris, A., and Liu, N.-S., "National Combustion Code: Parallel Implementation and Performance," NASA/TM—2000-209801, 2000.
13. Quealy, A., "National Combustion Code Parallel Performance Enhancements," NASA/CR—2002-211340.
14. Shih, T.-H., Povinelli, L.A., Liu, N.-S and Chen, K.-H., "Generalized Wall Function for Complex Turbulent Flows," NASA/TM—2000-209936, 2000.
15. Chien, K.Y., "Prediction of Boundary Layer Flows with a Low – Reynolds Number Turbulence Model," AIAA J., vol. 20, no. 1, pp. 33–38, 1982.
16. Shih, T.-H., Chen, K.-H., Liu, N.-S., Lumley, J.L., "Modeling of Turbulent Swirling Flows," NASA-TM–113112, Glenn Research Center, Cleveland, OH, 1998.
17. Shih, T.-H., Chen, K.-H., and Liu, N.-S., "A Non-Linear k-epsilon Model for Turbulent Shear Flows," AIAA Paper 98-3983, 1998.
18. Raju, M.S., "LSPRAY-II: A Lagrangian Spray Module," NASA/CR—2004-212958, Glenn Research Center, Cleveland, OH, 2004.
19. S. Venkateswaran, J.M. Weiss, C.L. Merkle, Y.-H. Choi, "Propulsion-Related Flowfields Using Preconditioned Navier-Stokes Equations," AIAA–92–3437, 1992.
20. S. Venkateswaran, C.L. Merkle, "Efficiency and Accuracy Issues in Contemporary CFD Algorithms," AIAA–2002–2251, 2002.
21. Chen, K.-H., Norris, A.T., Quealy, A., and Liu, N.-S., "Benchmark Test Cases for The National Combustion Code," 34th AIAA/ASME/SAE/ASEE Joint Propulsion Conference and Exhibit, Cleveland, OH, USA, July 13–15, 1998.
22. Iannetti, A., Tacina, R., Jeng, S.-M., and Cai, J., "Towards Accurate Prediction of Turbulent, Three-Dimensional, Recirculating Flows With the NCC," NASA/TM—2001-210761, AIAA–2001–0809, 2001.
23. T.-H. Shih, A. Norris, A. Iannetti, C.J. Marek, T.D. Smith, N.-S. Liu, and L.A. Povinelli (NASA, Glenn Research Center, Cleveland, OH, "A Study of Hydrogen/Air Combustor Using NCC," AIAA–2001–808, Aerospace Sciences Meeting and Exhibit, 39th, Reno, NV, Jan. 8–11, 2001.
24. Iannetti, A.C., Chen, K.-H., "An Initial Comparison of National Combustor Code Simulations Using Various Chemistry Modules With Experimental Gas Turbine Combustor Data," AIAA–2000–0330, 38th AIAA Aerospace Sciences Meeting, Reno, NV, USA, 2000.
25. C.K. Westbrook and F.L. Dryer, "Simplified Reaction Mechanisms for The Oxidation of Hydrocarbon Fuels In Flames," Combust. Sci. Technology, vol. 27, p. 31, 1981.
26. Penko, P.F.; Kundu, K.P.; Siow, Y.K.; and Yang, S.L., "A Kinetic Mechanism for Calculation of Pollutant Species in Jet-A Combustion," AIAA–2000–3035, 2000.
27. Kundu, K.P.; Penko, P.F.; and VanOverbeke, T.J., "A Practical Mechanism for Computing Combustion in Gas Turbine Engines," AIAA–99–2218, 1999.
28. Zeldovich, Y.B. The Oxidation of Nitrogen in Combustion and Explosions. Acta Physicochimica URSS 21. pp. 577–628, 1946.
29. Fennimore, C.P., 13th Symposium. (Int) Comb., p. 371, 1971.
30. Amsden, A.A., O'Rourke, P.J., and Butler, T.D., "KIVA-II: A computer program for chemically reactive flows with sprays," Report Number LA-11560-MS, Los Alamos National Lab, 1989.

31. Lefebvre, A.H., Atomization and Sprays, Hemisphere Publishing Corporation, New York, NY, USA, 1989.
32. El Banhawy, Y. and Whitelaw, J.H., "Calculation of the Flow Properties of a Confined Kerosene-Spray Flame," AIAA Journal, vol. 18, no. 12, pp. 1503–1510, 1980.
33. Schmidt, D.P., et al., "Pressure-Swirl Atomization in the Near Field," SAE Paper 1999-01-0496, 1999.
34. Chryssakis, C., et al., "Fuel Spray Simulation of High-Pressure Swirl-Injector for DISI Engines and Comparison With Laser Diagnostic Measurements," SAE Paper 2003-01-0007, 2003.
35. Raju, M.S., "Numerical Investigation of Various Atomization Models in the Modeling of a Spray Flame," NASA/CP—2005-214033, QSS Group, Glenn Research Center, Cleveland, OH, 2005.
36. Swanson, R.C., and Turkel, E., "Multistage Schemes with Multigrid for Euler and Navier – Stokes Equations," NASA-TP-3631, 1997.

REPORT DOCUMENTATION PAGE		Form Approved OMB No. 0704-0188

1. REPORT DATE *(DD-MM-YYYY)*	2. REPORT TYPE	3. DATES COVERED *(From - To)*
01-07-2010	Technical Memorandum	

4. TITLE AND SUBTITLE
Comparing Spray Characteristics from Reynolds Averaged Navier-Stokes (RANS) National Combustion Code (NCC) Calculations Against Experimental Data for a Turbulent Reacting Flow

5a. CONTRACT NUMBER

5b. GRANT NUMBER

5c. PROGRAM ELEMENT NUMBER

6. AUTHOR(S)
Iannetti, Anthony, C.; Moder, Jeffery, P.

5d. PROJECT NUMBER

5e. TASK NUMBER

5f. WORK UNIT NUMBER
WBS 561581.02.08.03.16.02

7. PERFORMING ORGANIZATION NAME(S) AND ADDRESS(ES)
National Aeronautics and Space Administration
John H. Glenn Research Center at Lewis Field
Cleveland, Ohio 44135-3191

8. PERFORMING ORGANIZATION REPORT NUMBER
E-17312

9. SPONSORING/MONITORING AGENCY NAME(S) AND ADDRESS(ES)
National Aeronautics and Space Administration
Washington, DC 20546-0001

10. SPONSORING/MONITOR'S ACRONYM(S)
NASA

11. SPONSORING/MONITORING REPORT NUMBER
NASA/TM-2010-216735

12. DISTRIBUTION/AVAILABILITY STATEMENT
Unclassified-Unlimited
Subject Categories: 07, 28, 34, and 64
Available electronically at http://gltrs.grc.nasa.gov
This publication is available from the NASA Center for AeroSpace Information, 443-757-5802

13. SUPPLEMENTARY NOTES

14. ABSTRACT
Developing physics-based tools to aid in reducing harmful combustion emissions, like Nitrogen Oxides (NOx), Carbon Monoxide (CO), Unburnt Hydrocarbons (UHC's), and Sulfur Dioxides (SOx), is an important goal of aeronautics research at NASA. As part of that effort, NASA Glenn Research Center is performing a detailed assessment and validation of an in-house combustion CFD code known as the National Combustion Code (NCC) for turbulent reacting flows. To assess the current capabilities of NCC for simulating turbulent reacting flows with liquid jet fuel injection, a set of Single Swirler Lean Direct Injection (LDI) experiments performed at the University of Cincinnati was chosen as an initial validation data set. This Jet-A/air combustion experiment operates at a lean equivalence ratio of 0.75 at atmospheric pressure and has a 4 percent static pressure drop across the swirler. Detailed comparisons of NCC predictions for gas temperature and gaseous emissions (CO and NOx) against this experiment are considered in a previous work. The current paper is focused on detailed comparisons of the spray characteristics (radial profiles of drop size distribution and at several radial rakes) from NCC simulations against the experimental data. Comparisons against experimental data show that the use of the correlation for primary spray break-up implemented by Raju in the NCC produces most realistic results, but this result needs to be improved. Given the single or ten step chemical kinetics models, use of a spray size correlation gives similar, acceptable results.

15. SUBJECT TERMS
Combustion; Computational fluid dynamics; Turbulent flow; Sprays

16. SECURITY CLASSIFICATION OF:			17. LIMITATION OF ABSTRACT	18. NUMBER OF PAGES	19a. NAME OF RESPONSIBLE PERSON
a. REPORT	b. ABSTRACT	c. THIS PAGE			STI Help Desk (email:help@sti.nasa.gov)
U	U	U	UU	48	19b. TELEPHONE NUMBER *(include area code)* 443-757-5802